A First Test of the Framed Standard Model against Experiment

José BORDES [1]
jose.m.bordes@uv.es
Departament Fisica Teorica and IFIC, Centro Mixto CSIC, Universitat de Valencia, Calle Dr. Moliner 50, E-46100 Burjassot (Valencia), Spain

CHAN Hong-Mo
h.m.chan@stfc.ac.uk
Rutherford Appleton Laboratory, Chilton, Didcot, Oxon, OX11 0QX, United Kingdom

TSOU Sheung Tsun
tsou@maths.ox.ac.uk
Mathematical Institute, University of Oxford, Radcliffe Observatory Quarter, Woodstock Road, Oxford, OX2 6GG, United Kingdom

Abstract

The framed standard model (FSM) is obtained from the standard model by incorporating, as field variables, the frame vectors (vielbeins) in internal symmetry space. It gives the standard Higgs boson and 3 generations of quarks and leptons as immediate consequences. It gives moreover a fermion mass matrix of the form: $m = m_T \boldsymbol{\alpha}\boldsymbol{\alpha}^\dagger$, where $\boldsymbol{\alpha}$ is a vector in generation space independent of the fermion species and rotating with changing scale, which has already been shown to lead, generically, to up-down mixing, neutrino oscillations and mass hierarchy. In this paper, pushing the FSM further, one first derives to 1-loop order the RGE for the rotation of $\boldsymbol{\alpha}$, and then applies it to fit mass and mixing data as a first test of the model. With 7 real adjustable parameters, 18 measured quantities are fitted, most (12) to within experimental error or to better than 0.5 percent, and the rest (6) not far off. (A summary of this fit can be found in Table 2 in the text.) Two notable features, both generic to FSM, not just specific to the fit, are: (i) that a theta-angle of order unity in the instanton term

[1]Work supported in part by Spanish MICINN and FEDER (EC) under grant FPA2011-23596 and GVPROMETEO2010-056

in QCD would translate via rotation into a Kobayashi-Maskawa phase in the CKM matrix of about the observed magnitude ($J \sim 10^{-5}$), (ii) that it would come out correctly that $m_u < m_d$, despite the fact that $m_t \gg m_b, m_c \gg m_s$. Of the 18 quantities fitted, 12 are deemed independent in the usual formulation of the standard model. In fact, the fit gives a total of 17 independent parameters of the standard model, but 5 of these have not been measured by experiment.

1 Introduction

We have been suggesting for some time that the standard model [1] be extended to include the frame vectors [2] in internal symmetry space as field variables (framons), i.e., in addition to the usual gauge boson and matter fermion fields, resulting in a theory we call the framed standard model (FSM) [3, 4]. The framons here are analogous to vierbeins in gravity [5] and their inclusion as fields in particle theory makes it closer in spirit to the theory of general relativity and may thus facilitate the eventual unification of the two. As for particle physics itself, the immediate attractions for so doing are:

- It gives the standard Higgs boson, which appears in FSM as the framon in the electroweak sector, both a theoretical basis and a geometrical significance.

- It gives to the theory, in addition to local gauge symmetry $su(3) \times su(2) \times u(1)$ of the standard model, a global counterpart, which we may call its "dual", $\widetilde{su}(3) \times \widetilde{su}(2) \times \tilde{u}(1)$, where the 3-fold symmetry $\widetilde{su}(3)$ can function as fermion generations [2], thus giving fermion generations a theoretical basis and geometrical significance as well.

- It gives a mass matrix for quarks and leptons of the form:

$$m = m_T \boldsymbol{\alpha}\boldsymbol{\alpha}^\dagger, \tag{1}$$

  where $\boldsymbol{\alpha}$, a vector in generation space, is "universal" (i.e., independent of the fermion species), and rotates with changing scale, properties which have been shown [8] to lead automatically both to up-down mixing and a hierarchical mass spectrum.

Practically, of course, the main attraction of substance is the last, since fermion mixing and mass hierarchy are two salient features imposed on to the standard model by experiment without, so far, any theoretical explanation of their origin. Indeed, it is the lack of such explanation that accounts for some two-thirds of the twenty-odd empirical parameters of the standard model as it is presently formulated, and any hint from anywhere towards an explanation would be welcome. Hence, an obvious question to ask as a first test of the FSM is whether it can indeed reproduce the mass and mixing parameters

[2] while $\widetilde{su}(2)$ is already known to represent up-down flavour [6] and $\tilde{u}(1)$ is $B - L$ [7].

seen in experiment [1, 9, 10]. Previously, the FSM has not been sufficiently developed to provide an answer. The purpose of this paper is to push it far enough to do so, and the result obtained so far appears to us very positive, as will be outlined in the next 2 paragraphs.

At tree-level in the FSM, the vector $\boldsymbol{\alpha}$ appearing in the fermion mass matrix (1) is constant, but corrections by framon loops make $\boldsymbol{\alpha}$ rotate with changing scale μ. Following standard procedure, the RGE for $\boldsymbol{\alpha}$ to 1-loop order is then derived. This equation depends on 5 real parameters: 1 coupling ρ and 3 integration constants a, R_I, θ_I, plus 1 fudge parameter k representing the dependence on μ of some quantities not yet covered by the present equation. However, to make contact with experiment, one needs to supply also the coefficients m_T appearing in (1), one for each fermion species, this being the mass of the heaviest state in that species, namely m_t, m_b, m_τ and m_{ν_3}. Of these the first 3 have been measured in experiment and are therefore non-adjustable, but the last m_{ν_3}, denoting the Dirac mass of the heaviest neutrino, is still unknown and has to be treated as a 6th parameter of the model. A 7th parameter is the theta-angle θ_{CP} from the instanton term in the QCD action which, in the FSM, translates by rotation [11, 8] into the Kobayashi-Maskawa phase of the CKM matrix. With these 7 parameters, then, the FSM is required to reproduce the mixing matrices of both quarks and leptons as well as their masses (except for neutrinos, the masses of which are likely to be subject to the see-saw mechanism [12] and thus require more assumptions beyond the basic tenets of the FSM).

For a chosen set of values for these 7 parameters, 23 quantities have been evaluated, of which 17 are regarded as independent in the standard model. This means that if a good fit to experiment is achieved for these quantities, then FSM would have succeeded in cutting the number of the relevant standard model parameters by more than half, from 17 to 7. Of the 23 quantities calculated, 18 have been measured in experiment. A comparison of the calculated values of these last 18 with data yields 10 within the stringent experimental errors ($< 1\sigma$), and 2 (m_μ, m_e, for which the minuscule experimental errors are beyond the accuracy of our calculation) to within less than 0.5 percent of the measured values. Of the other quantities 2 are close (1.5 and 1.7 σ respectively), while the remaining 4, though off, are still quite sensible and within striking distances of experiment. We consider that a pretty good score. The result is summarized in Table 2 in section 4, at which the reader is urged to have a glance before delving into the details which follow on how this result is obtained.

Now, a fermion mass matrix of the factorized form (1), with $\boldsymbol{\alpha}$ rotating with scale, may seem unusual and merits perhaps an immediate briefing on how it arises in the FSM. It is basically just a consequence of the framon action being invariant under the doubled symmetry $su(3) \times su(2) \times u(1)$ and $\widetilde{su}(3) \times \widetilde{su}(2) \times \tilde{u}(1)$ already stated. Because of this, framons in the FSM exist in 2 types, with the standard Higgs field appearing as the framon in the electroweak sector (the "weak framon"), together with a number of new scalar bosons as the "strong framon" fields. As usual, it is the Yukawa coupling of the Higgs boson which gives the fermion mass matrix, and it is the constraint of the doubled invariance on the Yukawa coupling of this "weak framon" field to fermions which gives a tree-level m of the particular form (1). At tree level, the vector $\boldsymbol{\alpha}$ is a constant, but $\boldsymbol{\alpha}$ is coupled to the strong vacuum through the framon self-interaction potential, again because of the doubled symmetry. Now, the strong vacuum itself is affected by radiative corrections via, in particular, the "strong framons", and these, being both coloured and dual-coloured, will change the orientation of the strong vacuum in $\widetilde{su}(3)$ or generation space and, like other radiative correction effects, this change would depend on the renormalization scale μ. This forces then the vector $\boldsymbol{\alpha}$ coupled to the strong vacuum also to change its orientation in generation space in a μ-dependent manner, or in other words, to rotate with changing μ, as asserted.

In the following section, we first briefly recall some earlier results essential for what follows and collect some tools to be used for calculating strong framon loops. Then in section 3 we shall derive to 1-loop order the RGE of rotation for $\boldsymbol{\alpha}$. And in section 4, we shall apply these RGE to calculate fermion masses and mixing parameters and to compare the result with existing data. In the last section (5) are remarks about, among other things, the range of validity of the derived rotation equation.

2 Essential Features and Tools

In this section we recall some properties of the FSM found earlier [4, 8], improving the notation wherever merited, while collecting the tools needed for the present paper.

The doubled invariance of the FSM under both the (local) gauge symmetry $G = su(3) \times su(2) \times u(1)$ and its "dual", the (global) symmetry $\tilde{G} = \widetilde{su}(3) \times \widetilde{su}(2) \times \tilde{u}(1)$, requires that its framon fields form a represen-

tation of $G \times \tilde{G}$. Minimality considerations in the number of fields to be introduced suggest then that the framons in FSM belong to the representation $(\mathbf{3}+\mathbf{2}) \times \mathbf{1}$ in G but to $\tilde{\mathbf{3}} \times \tilde{\mathbf{2}} \times \tilde{\mathbf{1}}$ in $\tilde{G}$ and that some of its components may be taken as dependent on others [3, 4], leaving just:

- a "weak framon" of the form:

$$\boldsymbol{\alpha} \otimes \boldsymbol{\phi} \tag{2}$$

  where $\boldsymbol{\alpha}$ is a triplet in $\widetilde{su}(3)$, which may be taken without loss of generality [4] as a real unit vector in generation space, but is constant in space-time, while $\boldsymbol{\phi}$ is an $su(2)$ doublet but Lorentz scalar field over space-time which has the same properties as, and may thus be identified with, the standard Higgs field;

- the "strong framon":

$$\boldsymbol{\beta} \otimes \boldsymbol{\phi}^{\tilde{a}}, \quad \tilde{a} = \tilde{1}, \tilde{2}, \tilde{3} \tag{3}$$

  where $\boldsymbol{\beta}$ is a doublet of unit length in $\widetilde{su}(2)$ space but constant in space-time, while $\boldsymbol{\phi}^{\tilde{a}}$ are 3 colour $su(3)$ triplet Lorentz scalar fields over space-time, which when taken as column vectors give a matrix Φ transforming by $su(3)$ transformation from the left but by $\widetilde{su}(3)$ transformations from the right.

The doubled invariance under $G \times \tilde{G}$ plus requirements of renormalizability restricts the framon self-interaction potential to the following form [3, 4]:

$$\begin{aligned} V[\boldsymbol{\alpha}, \boldsymbol{\phi}, \Phi] \;=\; & -\mu_W |\boldsymbol{\phi}|^2 + \lambda_W (|\boldsymbol{\phi}|^2)^2 \\ & -\mu_S \sum_{\tilde{a}} |\boldsymbol{\phi}^{\tilde{a}}|^2 + \lambda_S \left(\sum_{\tilde{a}} |\boldsymbol{\phi}^{\tilde{a}}|^2 \right)^2 + \kappa_S \sum_{\tilde{a},\tilde{b}} |\boldsymbol{\phi}^{\tilde{a}*} \cdot \boldsymbol{\phi}^{\tilde{b}}|^2 \\ & +\nu_1 |\boldsymbol{\phi}|^2 \sum_{\tilde{a}} |\boldsymbol{\phi}^{\tilde{a}}|^2 - \nu_2 |\boldsymbol{\phi}|^2 | \sum_{\tilde{a}} \alpha^{\tilde{a}} \boldsymbol{\phi}^{\tilde{a}}|^2. \end{aligned} \tag{4}$$

depending on 7 real coupling parameters. Notice in particular the term (with coefficient ν_2) which couples the vector $\boldsymbol{\alpha}$ from the weak framon in (2) to the strong framons in (3).

The vacuum is obtained, as usual, by minimizing the scalar potential, in this case the framon potential V in (4) . For μ_W, μ_S both positive, the

case that interests us, the minimum of V is degenerate in both the weak and strong sectors. In the weak sector the minimum is degenerate in the same way as in the standard model and little more needs to be said. It is the degeneracy in the strong sector which is at the centre of our present interest. Here it is found [4] that any chosen vacuum in the degenerate set can be cast by an appropriate choice of gauge into the following diagonal form:

$$\Phi_{\rm VAC} \longrightarrow \zeta_S V_0 = \zeta_S \begin{pmatrix} Q & 0 & 0 \\ 0 & Q & 0 \\ 0 & 0 & P \end{pmatrix}, \tag{5}$$

with:

$$P = \sqrt{(1+2R)/3}, \tag{6}$$

$$Q = \sqrt{(1-R)/3}, \tag{7}$$

$$R = \frac{\zeta_W^2 \nu_2}{2\kappa\zeta_S^2}, \tag{8}$$

where ζ_S and ζ_W are the vev's of the strong and weak framons respectively, and $\boldsymbol{\alpha}$, which is coupled to the vacuum, takes the value:

$$\boldsymbol{\alpha} \longrightarrow \boldsymbol{\alpha}_0 = \begin{pmatrix} 0 \\ 0 \\ 1 \end{pmatrix}. \tag{9}$$

Any other vacuum of the degenerate set can be obtained from this, but still in the same gauge, by applying a global $\widetilde{su}(3)$ transformation, say A^{-1}, to (5) from the right (and, simultaneously, the same A on $\boldsymbol{\alpha}_0$ from the left). The result, of course, will no longer be diagonal, but can be made diagonal again by applying an appropriate colour $su(3)$ transform from the left. However, for our present purpose, it is easier to keep to just one gauge choice so as to visualize better the change of the vacuum with the scale μ. In other words, we shall pick one vacuum of the degenerate set as the reference vacuum, and work throughout in the gauge where $\Phi_{\rm VAC}$ and $\boldsymbol{\alpha}$ at that reference vacuum take the forms (5) and (9) above.

We notice that the vacuum (5) has 2 equal eigenvalues. This is because the original $\widetilde{su}(3)$ in the strong sector is broken only by the vector $\boldsymbol{\alpha}$ from the weak framon. There is thus still a residual $\widetilde{su}(2)$ symmetry left in the system, namely the little group of $\boldsymbol{\alpha}$. This will be seen to play a prominent role in

constraining the manner that $\boldsymbol{\alpha}$ can rotate with changing scale, leading to physical consequences of much interest.

We are next interested in the quanta of fluctuations of the strong framon field about its vacuum expectation value (5) which, by analogy to the Higgs boson in the electroweak sector, we call the "strong Higgs" boson states. We shall see that it is the exchange of these latter states which will give rise to the rotation effect we seek. Again, the analysis can be carried out first around that particular chosen vacuum labelled by the superscript or subscript 0 and then extended to other vacua by an $\widetilde{su}(3)$ transformation. We choose to express these fluctuations as:

$$\Phi^0_{\rm VAC} + \delta\Phi = \Phi^0_{\rm VAC}(I + \epsilon S), \tag{10}$$

where S should be taken to be hermitian, as any anti-hermitian fluctuation would represent just a local gauge transformation under local $su(3)$. We choose for convenience also to expand S in terms of an orthonormal basis which is essentially just the unit matrix plus the Gell-Mann matrices, thus:

$$\delta\Phi = \sum_K V_K H_K, \tag{11}$$

where the H_K are then our strong Higgs states, and

$$\begin{aligned}
V_1 &= \begin{pmatrix} 1 & 0 & 0 \\ 0 & 0 & 0 \\ 0 & 0 & 0 \end{pmatrix} \\
V_2 &= \begin{pmatrix} 0 & 0 & 0 \\ 0 & 1 & 0 \\ 0 & 0 & 0 \end{pmatrix} \\
V_3 &= \begin{pmatrix} 0 & 0 & 0 \\ 0 & 0 & 0 \\ 0 & 0 & 1 \end{pmatrix} \\
V_4 &= \frac{1}{\sqrt{2}} \begin{pmatrix} 0 & 1 & 0 \\ 1 & 0 & 0 \\ 0 & 0 & 0 \end{pmatrix} \\
V_5 &= \frac{i}{\sqrt{2}} \begin{pmatrix} 0 & -1 & 0 \\ 1 & 0 & 0 \\ 0 & 0 & 0 \end{pmatrix}
\end{aligned}$$

$$
\begin{aligned}
V_6 &= \frac{1}{\sqrt{(P^2+Q^2)}}\begin{pmatrix} 0 & 0 & 0 \\ 0 & 0 & Q \\ 0 & P & 0 \end{pmatrix} \\
V_7 &= \frac{i}{\sqrt{(P^2+Q^2)}}\begin{pmatrix} 0 & 0 & 0 \\ 0 & 0 & -Q \\ 0 & P & 0 \end{pmatrix} \\
V_8 &= \frac{1}{\sqrt{(P^2+Q^2)}}\begin{pmatrix} 0 & 0 & Q \\ 0 & 0 & 0 \\ P & 0 & 0 \end{pmatrix} \\
V_9 &= \frac{i}{\sqrt{(P^2+Q^2)}}\begin{pmatrix} 0 & 0 & -Q \\ 0 & 0 & 0 \\ P & 0 & 0 \end{pmatrix} \\
&. \qquad (12)
\end{aligned}
$$

We shall need these matrices later to calculate strong Higgs loops.

By expanding V in (4) further to second order in the fluctuations of Φ about its vev, one obtains the tree-level mass matrix of the strong Higgs states H_K. This will be given only in the last section, for it will not be needed until then.

We turn next to the Yukawa couplings. Given the usual fermion fields in the standard model, one can write for the weak framon the following Yukawa term:

$$
\begin{aligned}
\mathcal{A}_{\rm YK}^{\rm weak} &= \sum_{[\tilde{a}][b]} Y_{[b]} \bar{\boldsymbol{\psi}}_{[\tilde{a}]} \alpha^{\tilde{a}} \boldsymbol{\phi} \tfrac{1}{2}(1+\gamma_5)\psi^{[b]} + \sum_{[\tilde{a}][b]} Y'_{[b]} \bar{\boldsymbol{\psi}}_{[\tilde{a}]} \alpha^{\tilde{a}} \boldsymbol{\phi}^c \tfrac{1}{2}(1+\gamma_5)\psi'^{[b]} \\
&\quad + \text{h.c.} \qquad (13)
\end{aligned}
$$

for leptons (similarly for quarks), where the indices $[\tilde{a}]$ and $[b]$ just label copies of identical $\widetilde{su}(3)$ singlet fields. As usual, the tree-level quark and lepton mass matrices are obtained by replacing the Higgs field $\boldsymbol{\phi}$ by its vev ζ_W, giving rank-1 matrices, which, by a harmless relabelling of the singlet right-handed fields, can all be cast into the form (1) above, with $m_T = \zeta_W \rho_W$ where ρ_W is the Yukawa coupling strength. The vector $\boldsymbol{\alpha}$ in $\widetilde{su}(3)$ generation space is universal because it comes originally from the weak framon (2) and so is independent of the fermion field to which the framon is coupled.

Similarly, one can consider a Yukawa coupling of the strong framon field (3) but this needs more discussion and we shall save it for the next section

where it will be the centre of attention for deriving the RGE for the rotation of $\boldsymbol{\alpha}$.

Once one knows $\boldsymbol{\alpha}$ as a function of the scale μ, then the conclusions of earlier analyses [8] allow one to calculate the masses and state vectors in generation space of the various quark and lepton states by solving the coupled equations, for the U-quarks, for example:

$$\begin{aligned} \mathbf{t} &= \boldsymbol{\alpha}(\mu = m_t); \\ \mathbf{c} &= \mathbf{u} \times \mathbf{t}; \\ \mathbf{u} &= \frac{\boldsymbol{\alpha}(\mu = m_t) \times \boldsymbol{\alpha}(\mu = m_c)}{|\boldsymbol{\alpha}(\mu = m_t) \times \boldsymbol{\alpha}(\mu = m_c)|}, \end{aligned} \tag{14}$$

and:

$$\begin{aligned} m_t &= m_U, \\ m_c &= m_U |\boldsymbol{\alpha}(\mu = m_c) \cdot \mathbf{c}|^2, \\ m_u &= m_U |\boldsymbol{\alpha}(\mu = m_u) \cdot \mathbf{u}|^2, \end{aligned} \tag{15}$$

with $m_U = m_t$ to be taken from experiment. The values m_t, m_c, m_u are then the masses, and $\mathbf{t}, \mathbf{c}, \mathbf{u}$ (in the absence of instantons in QCD, i.e., when $\theta_{CP} = 0$) are the state vectors of t, c, u.

However, when there are instantons, as in general there will be, and $\theta_{CP} \neq 0$, then CP for quarks will have to be redefined by a chiral transformation to eliminate θ_{CP} from the QCD action (i.e., to "solve the strong CP problem") so as to restore CP-invariance to the strong sector [13]. (Such chiral transformations are allowed in the FSM because the quark mass matrix (1) has zero eigenvalues [14].) The state vectors then become:

$$\begin{aligned} \tilde{\mathbf{t}} &= \boldsymbol{\alpha}(\mu = m_t), \\ \tilde{\mathbf{c}} &= \cos\omega_U \boldsymbol{\tau}(\mu = m_t) - \sin\omega_U \boldsymbol{\nu}(\mu = m_t) e^{-i\theta_{CP}/2}, \\ \tilde{\mathbf{u}} &= \sin\omega_U \boldsymbol{\tau}(\mu = m_t) + \cos\omega_U \boldsymbol{\nu}(\mu = m_t) e^{-i\theta_{CP}/2}, \end{aligned} \tag{16}$$

where $\boldsymbol{\tau}$ is the unit tangent vector to the trajectory of $\boldsymbol{\alpha}$ at $\mu = m_t$, $\boldsymbol{\nu} = \boldsymbol{\alpha} \times \boldsymbol{\tau}$ is the binormal and $\cos\omega_U = \mathbf{c} \cdot \boldsymbol{\tau}$. These formulae differ from those of (14) essentially in an extra phase rotation $e^{-i\theta_{CP}/2}$ on the binormal $\boldsymbol{\nu}$.

Similar considerations hold also for D-quarks, which together with the above then give the CKM matrix as:

$$V_{CKM} = \begin{pmatrix} \tilde{\mathbf{u}} \cdot \tilde{\mathbf{d}} & \tilde{\mathbf{u}} \cdot \tilde{\mathbf{s}} & \tilde{\mathbf{u}} \cdot \tilde{\mathbf{b}} \\ \tilde{\mathbf{c}} \cdot \tilde{\mathbf{d}} & \tilde{\mathbf{c}} \cdot \tilde{\mathbf{s}} & \tilde{\mathbf{c}} \cdot \tilde{\mathbf{b}} \\ \tilde{\mathbf{t}} \cdot \tilde{\mathbf{d}} & \tilde{\mathbf{t}} \cdot \tilde{\mathbf{s}} & \tilde{\mathbf{t}} \cdot \tilde{\mathbf{b}} \end{pmatrix}, \tag{17}$$

which will in general be complex with a nonzero CP-violating KM phase depending on θ_{CP}, the strong CP problem having been transmuted by FSM to become the KM phase [11].

Leptons, on the other hand, are not involved, as far as one knows, when $\theta_{CP} \neq 0$, so that a solution of the leptonic version of the equations (14) and (15) may already give the state vectors, leading to a real PMNS mixing matrix, although there is also no compulsion for this being so. We shall leave the question open, to be explored later when fitting data. The solution of the same equations will give also the masses of the charged leptons and the "Dirac masses" of the neutrinos, but the physical masses of the neutrinos will likely be given by some see-saw mechanism and cannot be obtained in the present FSM without further assumptions.

With the above formulae, one will be able to calculate the masses and mixing parameters for both quarks and leptons (except physical masses for neutrinos) once one knows the trajectory for $\boldsymbol{\alpha}$.

3 RGE for the Rotation of $\boldsymbol{\alpha}$

What we are after in this section is the scale-dependence of the vector $\boldsymbol{\alpha}$ which appears in the mass matrix (1). Strictly speaking, $\boldsymbol{\alpha}$, being a vector in $\widetilde{su}(3)$ space, carries only global $\tilde{a}$ indices and cannot emit or absorb framon or gauge boson quanta which carry local $su(3)$ indices, and are thus not subject directly to radiative corrections by framon or gauge boson loops. However, as is seen in (4), $\boldsymbol{\alpha}$ is coupled to the strong vacuum because of the required double invariance on the framon action, so that if the strong vacuum, which is subject to radiative corrections, moves with scale, so must $\boldsymbol{\alpha}$ move as well. Another way of putting it is as follows. The strong vacuum in FSM is degenerate, different elements in the degenerate set being related by $\widetilde{su}(3)$ transformations. So if the strong vacuum moves from one element to another within this degenerate set, an $\widetilde{su}(3)$ transformation, say A, is induced, and $\boldsymbol{\alpha}$, being a vector in $\widetilde{su}(3)$ will be transformed by A as well, i.e., will rotate.

That being the case, our attention is now directed towards the strong vacuum in FSM. Information on how the strong vacuum moves with scale can be obtained in principle from the RGE of any field quantity which depends on the strong vacuum. Our first choice, mainly for historical reasons, fell on a Yukawa-type coupling, on which we have had some experience in connection with the mass matrix rotation problem.

However, it is not immediately obvious how to construct a Yukawa coupling from the strong framon field with the fermion fields that we have inherited from the standard model, where all left-handed fields are $su(2)$ doublets and all right-handed fields are $su(2)$ singlets. The strong framon Φ, being a scalar field, couples a left-handed to a right-handed fermion field but, being itself an $su(2)$ singlet, cannot neutralize the $su(2)$ indices of the left-handed fields, as the ordinary $su(2)$-doublet Higgs field $\boldsymbol{\phi}$ does, to make the Yukawa coupling an $su(2)$ invariant. One can nevertheless construct solely from available right-handed fermion fields invariant couplings of the following form:

$$\mathcal{A}_{\rm YK}^{\rm strong} = \sum_{[b]} Z_{[b]} \left[\bar{\psi}^a_R \boldsymbol{\phi}_a\right]^C_{\tilde{a}} \alpha^{\tilde{a}}_Y \psi^{[b]}_R + \text{h.c.}, \tag{18}$$

where C represents charge conjugation, and $\boldsymbol{\alpha}_Y$ is some (it can be any) vector in dual colour $\widetilde{su}(3)$ space. We notice that the quantity inside the square bracket in the above expression can be entirely neutral so that the construction is faintly reminiscent of the manner that the Majorana mass term for neutrinos is constructed. But it can also be written with a ψ'

$$(\bar{\psi}')^a \tfrac{1}{2}(1+\gamma_5) = (\bar{\psi}^a_R)^C \tag{19}$$

as:

$$\mathcal{A}_{\rm YK}^{\rm strong} = \sum_{[b]} Z_{[b]} \bar{\psi}'^a \boldsymbol{\phi}^*_a \cdot \boldsymbol{\alpha}_Y \frac{1}{2}(1+\gamma_5)\psi^{[b]} + \text{h.c.}, \tag{20}$$

of the Yukawa type we seek.[3]

It has yet to be worked out explicitly which of the fermion fields can have couplings of the form (18), together with all the details of the consequences that these couplings could lead to. These can be quite intriguing and intricate and cannot be adequately dealt with in the present paper in any case. But, as far as the effects of renormalization on the strong vacuum is concerned, which is what interests us here, it will not matter, so long as the said coupling exists.

This coupling is particularly convenient for our purpose. First, on replacing the strong framon field by its vacuum expectation value, it gives a mass matrix $\mathbf{m}$ depending on the vev of Φ, and any change in $\mathbf{m}$ from renormalization will give information on the associated change in the vev of Φ,

[3]This is superior, we think, to an alternative interpretation of the same expression as an effective coupling for quarks given before in [4], the present one being a renormalizable vertex in the fundamental fields.

hence also the change in $\boldsymbol{\alpha}$ that we seek. Secondly, the coupling contains also the information on how the strong framons Φ, or equivalently the (strong) Higgs states H_K, couple to the fermion states, and allows immediately the calculation of H_K loops. We recall that it is the change in orientation of $\boldsymbol{\alpha}$ (hence also the strong vacuum) in $\widetilde{su}(3)$ space that is wanted, and the strong framons or the H_K, being the only particles in the theory which carry $\widetilde{su}(3)$ indices, are the ones that would affect most directly the change in orientation.

The information obtained from (20) alone on the rotation of $\boldsymbol{\alpha}$ will not be exhaustive, nor necessarily more complete than that which can be obtained potentially from the RGE of some other quantity. Nevertheless, it will be seen to be already enough for our immediate needs. An investigation on the RGE of some other quantities has started, which might yield further information on the scale dependence of $\boldsymbol{\alpha}$. This should not, however, be in contradiction with that obtained here from (20) if the theory is self-consistent, but should rather supplement whatever might still be missing.

Let us now choose as reference vacuum that which has its $\boldsymbol{\alpha}$ the same as the $\boldsymbol{\alpha}_Y$ appearing in (20), and work in the gauge where the vacuum expectation values of Φ and of $\boldsymbol{\alpha}$ have the forms (5) and (9).

Anticipating the result that the vacuum will change with scale under renormalization, we shall need to work with a general vacuum related to the reference vacuum by an $\widetilde{su}(3)$ transformation A, though still in the reference gauge. For deriving the renormalization group equations we seek, it is sufficient to take A real, i.e., as a 3×3 orthogonal matrix. Expanding then Φ^* up to first order in its fluctuations about the vacuum $\Phi^0_{\rm VAC} A^{-1}$, thus:

$$\Phi^* = \zeta_S V_0 A^{-1} + \sum_K V_K^* A^{-1} H_K, \tag{21}$$

we obtain, on substituting into (20), and introducing for short:

$$\mathbf{v} = A^{-1} \boldsymbol{\alpha}_0, \tag{22}$$

to zeroth order, a (strong fermion) mass term:

$$\mathcal{A}^{\rm strong}_{\rm mass} = \sum_{a,[b]} \bar{\psi'}^a \mathbf{m}_{a[b]} \tfrac{1}{2}(1+\gamma_5) \psi^{[b]} + \text{h.c.}, \tag{23}$$

with the (strong fermion) mass matrix $\mathbf{m}$ as:

$$\mathbf{m}_{a[b]} = \zeta_S (V_0 \mathbf{v})_a Z_{[b]}, \tag{24}$$

and to first order in the fluctuations, a (strong) fermion-Higgs coupling term:

$$\mathcal{L}_Y^{\rm strong} = \sum_{a,[b]} \bar{\psi}'^a \left(\sum_K \Gamma_K H_K \right)_{a[b]} \tfrac{1}{2}(1+\gamma_5)\psi^{[b]} + \text{h.c.}, \tag{25}$$

with

$$\Gamma_K = V_K^* |\mathbf{v}\rangle\langle Z|. \tag{26}$$

Given the (strong) fermion-Higgs couplings Γ_K, the RGE for the (strong) fermion mass matrix $\mathbf{m}$ in (23) can be derived along standard lines. Following [16, 17, 18], the Feynman diagrams to 1-loop level which give corrections to the Yukawa coupling or the mass matrix and the RGE for $\mathbf{m}$ are listed below:

$(\Gamma_K \Gamma_K^\dagger)\mathbf{m} \,+\, \mathbf{m}\,(\Gamma_K^\dagger \Gamma_K)$

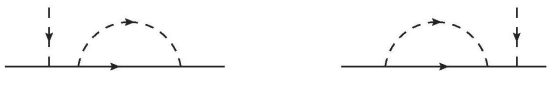

$\Gamma_K\, \mathbf{m}^\dagger\, \Gamma_K$

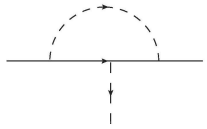

$\Gamma_K\, \mathtt{Tr}\,(\Gamma_K\, \mathbf{m}^\dagger \,+\, \mathbf{m}\, \Gamma_K^\dagger)$

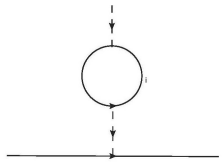

Summing the contributions, the RGE of the mass matrix is obtained as:

$$16\pi^2 \frac{d\,\mathbf{m}}{d\,t} = \sum_K \left\{ \frac{1}{2} \left[(\Gamma_K \Gamma_K^\dagger)\mathbf{m} + \mathbf{m}(\Gamma_K^\dagger \Gamma_K) \right] + 2\Gamma_K \mathbf{m}^\dagger \Gamma_K + \Gamma_K \mathtt{Tr}(\Gamma_K \mathbf{m}^\dagger + \mathbf{m}\Gamma_K^\dagger) \right\} \tag{27}$$

where the sum K runs over the whole set of Γ_K's in (26) with V_K listed in (12). This implicitly assumes that we are using the RGE at scales above the masses of all the (strong) Higgs states H_K.

Next, performing the calculation of the different terms for Γ_K in (26) and V_K in (12), one has:

$$\begin{aligned}
\Gamma_K\,\mathtt{Tr}\,(\Gamma_K\,\mathbf{m}^\dagger \;+\; \mathbf{m}\,\Gamma_K^\dagger) \;&=\; (\Gamma_K\,\Gamma_K^\dagger)\,\mathbf{m} \,+\, \Gamma_K\,\mathbf{m}^\dagger\Gamma_K \\
\sum_K (\Gamma_K\,\Gamma_K^\dagger)\,\mathbf{m} \;&=\; \rho_S^2\,\mathrm{diag}\,\Big(1-v_3^2\,+\,\frac{2Q^2}{P^2+Q^2}\,v_3^2, \\
&\qquad 1-v_3^2\,+\,\frac{2Q^2}{P^2+Q^2}\,v_3^2,\; v_3^2\,+\,\frac{2P^2}{P^2\,+\,Q^2}\,(1-v_3^2)\Big)\,\mathbf{m} \\
\mathbf{m}\sum_K (\Gamma_K^\dagger\,\Gamma_K) \;&=\; \rho_S^2\,\left(\frac{1}{P^2+Q^2}+\frac{3}{P^2+Q^2}(P^2(1-v_3^2)\,+\,Q^2\,v_3^2)\right)\mathbf{m} \\
\sum_K \Gamma_K\,\mathbf{m}^\dagger\,\Gamma_K \;&=\; \rho_S^2\,\Big\{\mathrm{diag}\,\Big(1-v_3^2,\,1-v_3^2,\,v_3^2\Big)\,+ \\
&\qquad +\,\frac{2}{P^2+Q^2}\,\mathrm{diag}\,\Big(P^2\,v_3^2,\,P^2\,v_3^2,\,Q^2\,(1-v_3^2),\Big)\Big\}\,\mathbf{m}
\end{aligned} \tag{28}$$

Here

$$\rho_S^2 = \langle \mathbf{Z}|\mathbf{Z}\rangle, \tag{29}$$

is the Yukawa coupling strength in (20).

Adding the contributions, one has then

$$\frac{d\,\mathbf{m}}{d\,t} \;=\; \mathrm{diag}\,(\gamma,\gamma,\beta)\;\mathbf{m} \tag{30}$$

where

$$\gamma = \frac{3\rho_S^2}{16\pi^2}\left(2+\frac{R}{2(2+R)}\right);\qquad \beta = \frac{3\rho_S^2}{16\pi^2}\left(2-\frac{R}{2+R}\right). \tag{31}$$

Notice that the mass matrix $\mathbf{m}$ defined in (24) being of rank 1, the matrix multiplying $\mathbf{m}$ on the right-hand side in (30) is not unique, and may even be nondiagonal. The present diagonal choice, however, is particularly convenient for our purpose.

The equation (30) can be rewritten using (24) in terms of the unit vector $\mathbf{v}$ as follows:

$$\frac{d}{dt}\;(\rho_S\zeta_S V_0\mathbf{v}) = \begin{pmatrix} \gamma & & \\ & \gamma & \\ & & \beta \end{pmatrix}(\rho_S\zeta_S V_0\mathbf{v}) \tag{32}$$

or else, even more explicitly, in terms of its components as:

$$\frac{\dot{v}_1}{v_1} = \gamma - \frac{\dot{Q}}{Q} - \left[\frac{\dot{\zeta}_S}{\zeta_S} + \frac{\dot{\rho_S}}{\rho_S} + (QCD)\right], \tag{33}$$

$$\frac{\dot{v}_2}{v_2} = \frac{\dot{v}_1}{v_1}, \tag{34}$$

$$\frac{\dot{v}_3}{v_3} = \beta - \frac{\dot{P}}{P} - \left[\frac{\dot{\zeta}_S}{\zeta_S} + \frac{\dot{\rho_S}}{\rho_S} + (QCD)\right], \tag{35}$$

where we have inserted a term (QCD) in each component for the possible gluon-loop contribution to the renormalization effect which, being non-perturbative at low energies and therefore unknown, has so far been ignored. An important point to note here is that on the right-hand sides of the equations (33)—(35), only the terms γ or β and $\dot{Q}/Q$ or $\dot{P}/P$ depend on the component. This means that if it were not for the presence of these terms, the vector $\mathbf{v}$ would not rotate with scale at all. For example, the terms denoted by (QCD) coming from gluon-loops will only change the normalization of $\mathbf{v}$, not its orientation, and will not by themselves lead to any rotation, confirming the earlier statement that only strong framon or H_K-loops will give rotation directly. However, given now that the vector $\mathbf{v}$ has to remain a unit vector, the normalization-changing terms inside the square brackets, though identical for all components, will have an indirect effect on the manner that $\mathbf{v}$ rotates. In what follows, we choose to write the common quantity inside the square brackets in (33) and (35) as:

$$[\,\cdots\,] = -\frac{k}{2}\frac{\dot{R}}{R}, \tag{36}$$

for reasons which will soon be made apparent.

The equation (34) can be integrated to give:

$$v_2 = \text{constant} \times v_1. \tag{37}$$

This simple result comes just from the fact that the matrix on the right of (30) has 2 equal eigenvalues, which is itself the consequence of the residual $\widetilde{su}(2)$ symmetry already mentioned. It will be seen to have a significant role in determining the physical outcome.

Further, for easier manipulation, the equation (33) can be replaced by:

$$\beta v_3^2 + \gamma(1 - v_3^2) = -\frac{k}{2}\frac{\dot{R}}{R} + \frac{\dot{P}}{P}v_3^2 + \frac{\dot{Q}}{Q}(1 - v_3^2), \tag{38}$$

which is derived via (33)—(35) from the condition that $\mathbf{v}$ is a unit vector.

Next, the equations (35), (37) and (38) on the components of $\mathbf{v} = A^{-1}\boldsymbol{\alpha}_0$ can be translated into conditions on the components of the vector $\boldsymbol{\alpha} = A\boldsymbol{\alpha}_0$ of our actual interest using the relations:

$$\begin{aligned} \alpha^{\tilde{1}} &= \frac{v_1 v_3}{\sqrt{(v_2)^2 + (v_3)^2}}, \\ \alpha^{\tilde{2}} &= \frac{v_2}{\sqrt{(v_2)^2 + (v_3)^2}}, \\ \alpha^{\tilde{3}} &= v_3. \end{aligned} \tag{39}$$

From their definitions in terms of the orthogonal transformation A, one sees that $\mathbf{v}$ is the third row and $\boldsymbol{\alpha}$ the third column of the matrix representing A in the basis we are using, and one would not normally expect any relationship between them. The above relations arise here, however, again because of the residual symmetry which is the little group of $\boldsymbol{\alpha}_0$. A rotation about $\boldsymbol{\alpha}_0$ as axis has no effect on $\mathbf{v}$, so that in terms of suitably chosen Euler angles θ_i and the corresponding rotations R_i, $i = 1, 2, 3$, we can write

$$A^{-1} = R_1^{-1} R_2^{-1} R_3^{-1} \tag{40}$$

and

$$\mathbf{v} = A^{-1}\boldsymbol{\alpha}_0 = R_1^{-1} R_2^{-1}\boldsymbol{\alpha}_0. \tag{41}$$

The RGE's we have derived tell us how $\mathbf{v}$ rotates with μ, i.e., how θ_1 and θ_2 change with μ, but give no μ-dependent constraint on θ_3. Working out θ_1 and θ_2 in terms of $\mathbf{v}$ and substituting into:

$$\boldsymbol{\alpha} = R_3 R_2 R_1 \boldsymbol{\alpha}_0, \tag{42}$$

then gives the above relationship (39), apart from premultiplication by an arbitrary rotation R_3 about $\boldsymbol{\alpha}_0$ as axis, which however, being μ-independent, is immaterial for what follows.

Applying then (39) to the equations (35), (37) and (38) gives the equations in terms of $\boldsymbol{\alpha}$ respectively as:

$$\frac{\dot{\alpha}^{\tilde{3}}}{\alpha^{\tilde{3}}} = \beta - \frac{\dot{P}}{P} + \frac{k}{2}\frac{\dot{R}}{R}, \tag{43}$$

$$\frac{\alpha^{\tilde{2}}\alpha^{\tilde{3}}}{\alpha^{\tilde{1}}} = \text{constant}, \tag{44}$$

and

$$\beta(\alpha^{\tilde{3}})^2 + \gamma[1-(\alpha^{\tilde{3}})^2] = \frac{\dot{P}}{P}(\alpha^{\tilde{3}})^2 + \frac{\dot{Q}}{Q}[1-(\alpha^{\tilde{3}})^2] - \frac{k}{2}\frac{\dot{R}}{R}. \tag{45}$$

Introducing next polar co-ordinates for $\boldsymbol{\alpha}$:

$$\boldsymbol{\alpha} = \begin{pmatrix} \sin\theta\cos\phi \\ \sin\theta\sin\phi \\ \cos\theta \end{pmatrix}, \tag{46}$$

we obtain the RGE for rotation in the form we shall apply [4]:

$$\dot{R} = -\frac{3\rho_S^2}{16\pi^2}\frac{R(1-R)(1+2R)}{D}\left(4 + \frac{R}{2+R} - \frac{3R\cos^2\theta}{2+R}\right) \tag{47}$$

$$\dot{\theta} = -\frac{3\rho_s^2}{32\pi^2}\frac{R\cos\theta\sin\theta}{D}\left(12 - \frac{6R^2}{2+R} - \frac{3k(1-R)(1+2R)}{2+R}\right) \tag{48}$$

and

$$\cos\theta\tan\phi = a, \tag{49}$$

with a constant, and

$$D = R(1+2R) - 3R\cos^2\theta + k(1-R)(1+2R). \tag{50}$$

4 Fit to Experimental Data

We shall describe and analyse the fit in some detail because, given the relative novelty of the FSM mechanism, it is important not just to get a fit but also to understand how it comes about.

The information provided by the renormalization group equations derived above which govern the rotation trajectory for $\boldsymbol{\alpha}$ divides conveniently into two parts, one (A) specifying the shape of the curve, say Γ, traced out by $\boldsymbol{\alpha}$

[4]The first two of these equations supersede and replace the equations (76) and (77) in [4]. The earlier equations were derived before the problem was fully understood and, though enough for the then immediate purpose of showing that $\boldsymbol{\alpha}$ rotates, contain some errors and omissions in details. This new systematic approach corrects an important sign error, and fills in some logical steps as well as the strong framon tadpole contribution missing in the earlier attempt.

on the unit sphere as it moves with scale, and the other (B) specifying the scale-dependent speed at which it moves along that curve.

(A) The shape of Γ is given by the equation (49) which depends on only 1 parameter, the integration constant a. Besides, although it was derived above explicitly only at the 1-loop level, it was seen in (37) to be a consequence of the vacuum being invariant under an $\widetilde{su}(2)$ subgroup, namely the little group of $\boldsymbol{\alpha}$, of the global dual colour symmetry $\widetilde{su}(3)$, ultimately traceable to the same invariance in the framon potential V in (4). One expects it to hold therefore even at higher-loop levels.

A plot of Γ for several values of a is shown in Figure 1, where it is seen that it has a sharp bend near $\theta = \pi/2, \phi = 0$, with the bend becoming sharper at smaller magnitudes of a [5]. In other words, it has considerable geodesic curvature somewhere along its length, which, as noted earlier [19, 8], is essential for the Cabibbo angle (i.e., $V_{us} \sim V_{cd}$ in the CKM matrix) to acquire the sizeable value it is known experimentally to possess. It is also necessary to give nonzero though still small values to the corner elements (V_{ub}, V_{td}) of the CKM matrix which arise only from second-order curvature terms which are torsion-like [20]. Furthermore, one notes that the geodesic curvature changes sign at $\theta = 0$, which will be seen later to lead correctly to the result $m_u < m_d$. This last, of course, is a physically crucial fact, though a surprising one, given that in both the 2 heavier generations, $m_t \gg m_b, m_c \gg m_s$, and is thus an elusive target for model builders.

(B) The scale-dependent speed at which $\boldsymbol{\alpha}$ moves along the curve Γ is prescribed by the equations (47) and (48). It is much less precisely predicted by the FSM than is the shape of Γ, being known at present only to 1-loop, and even at that level depends on 3 parameters, namely the Yukawa coupling strength ρ_S and 2 integration constants, say R_I and θ_I at some chosen initial scale μ_I. Even more seriously, it depends also on a quantity inside the square brackets in (33) and (35) which are unknown and may not even be calculable at present, and in the equations (47) and (48) are just lumped together in the unknown function $k(\mu)$.

Still, there are discernible in (47) and (48) certain features which lead to immediate physical consequences, having perhaps a more general validity

[5] The sign of a, which is directly related to the overall sign of the geodesic curvature, is immaterial, as this just fixes the relative orientation of the curve to the sphere.

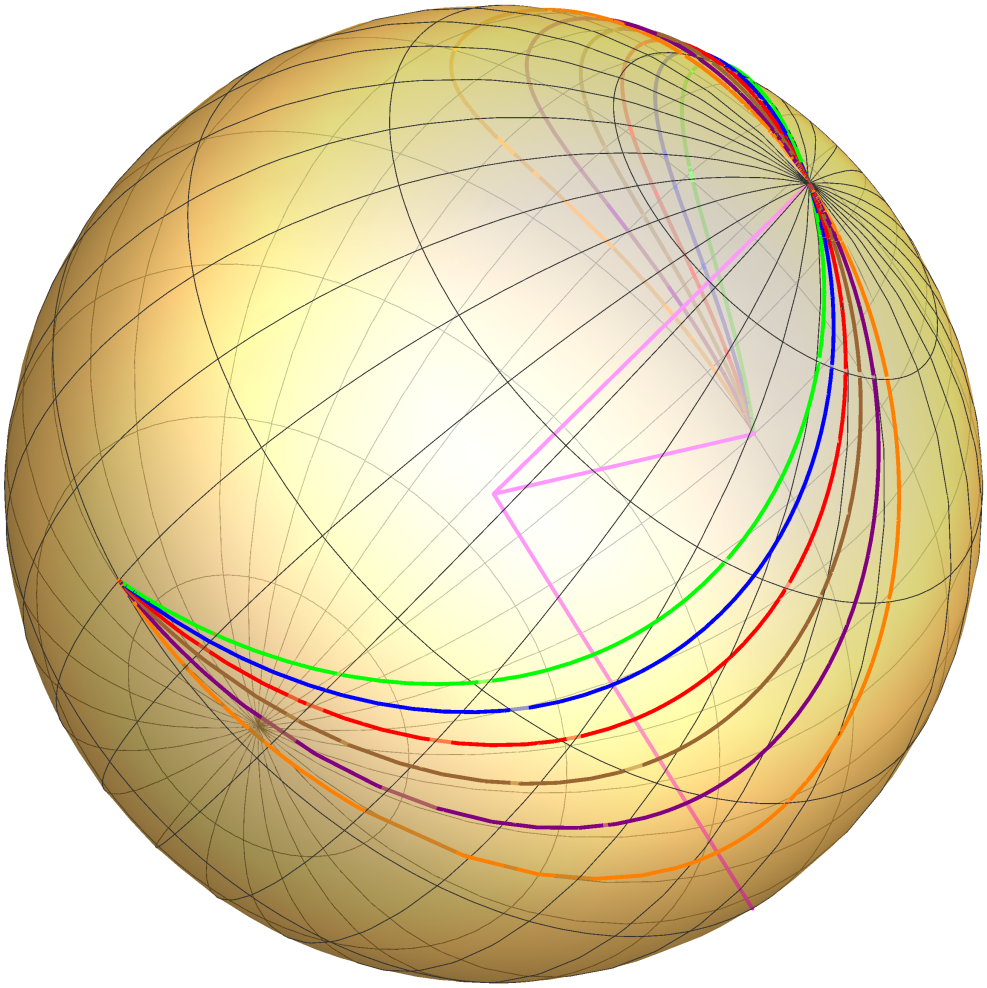

Figure 1: The curve Γ traced out by the vector $\boldsymbol{\alpha}$ on the unit sphere in generation space for various values of the integration constant a, decreasing in magnitude from $a = -0.6$ in green to $a = -0.1$ in orange.

beyond the 1-loop level at which they are derived. Thus first, one notices that in both equations there is a factor R on the right-hand side in front, which means that both $\dot{R}$ and $\dot{\theta}$ will vanish at $R = 0$, or in other words, that there will be a fixed point at infinite scale μ at $R = 0$. As the scale lowers from ∞, therefore, the change in θ, or rotation, will accelerate, at least initially for high mass scales. Now, since in the FSM, the masses of the second generation relative to the heaviest, are consequences just of rotation and would increase for increasing rotation speed, it follows immediately from this that $m_c/m_t < m_s/m_b < m_\mu/m_\tau$, simply by virtue of the fact that $m_t > m_b > m_\tau$, i.e., at least if the acceleration effect persists that far.

However, there is yet another reason why the noted acceleration would persist beyond the immediate vicinity of the fixed point at $\mu = \infty$. On the right-hand side of (48), there is a factor $\sin\theta$ which would seem at first sight to make $\dot{\theta}$ vanish at $\theta = 0$ so that θ cannot then change any further. Surprisingly, this is not true, at least for the type of solutions which is of interest to us, for which the denominator D also vanishes at $\theta = 0$. This cancellation is quite intriguing and deserves some examination. One notices that D being dependent on both θ and R, its behaviour as $\theta \to 0$ will depend on the direction on the θR-plane in which that limit point is approached. It turns out that for the solutions of interest to us, the approach is from near the θ-direction around $R = 1$ so that D becomes effectively just $3\sin^2\theta$ for whatever value of k at the corresponding value of μ. In other words, D not only cancels off the original zero in the numerator but even makes $\dot{\theta}$ virtually infinite. Or that the initial acceleration near the fixed point at $\mu = \infty$ not only will persist until but will indeed become enhanced around the value of μ at which θ crosses zero. As to what value of μ at which this happens, and why the solutions of interest to us should choose to approach $\theta = 0$ this way, it will have to be explained later after one has had some experience in fitting data. For the moment, one will only note that since up-down mixing in the FSM is also a consequence of rotation, the fact that rotation will continue to accelerate at low scales would immediately imply that the mixing angles for leptons will in general be bigger than the corresponding ones for quarks, as are actually seen in experiment, simply because quarks are heavier than leptons in general.

These implications come only from the 2 kinematic factors, R and D in the RGE (47) and (48), one in the numerator and one in the denominator, which seem to have little to do with the 1-loop approximation from which the RGE are here derived. We are thus hopeful that they might persist even

	Expt (September 2014)	Input value
m_t	$173.07 \pm 0.52 \pm 0.72$ GeV	173.5 GeV
m_b	4.18 ± 0.03 GeV	4.18 GeV
m_τ	1776.82 ± 0.16 MeV	1.777 GeV

Table 1: Masses of t, b and τ used in our calculation.

at higher loops.

With these qualitative observations made, we are now ready to proceed to a quantitative analysis so as to ascertain whether the derived renormalization group equations (49), (47) and (48) do actually measure up to expectation for the description of experimental data. These equations depend on the Yukawa coupling strength ρ_S or $c = \rho_S^2/16\pi^2$, and an at present unknown function $k(\mu)$. Clearly, one can do little phenomenologically with an unknown function. We shall therefore fudge it and replace it with a constant k, basically assuming that the quantity inside the square brackets in (33) and (35) has a scale-dependence similar to $\dot{R}/R$, and take k as another parameter to be fitted to experiment. One can hope that future renormalization studies of quantities other than the Yukawa coupling studied here may yield new information on the function $k(\mu)$. Here, we can only hope that replacing it by a constant may not be too drastic, since the quantity in square brackets, as argued above, are secondary effects affecting rotation only indirectly through the normalization of the unit vector $\mathbf{v}$.

Assuming some values of c and k, together with some initial values for the 2 variables R, θ at some convenient scale μ_I, one can easily integrate numerically the equations to obtain R and θ as functions of μ, from which the other polar angle ϕ can be obtained by solving (49) for Γ. Hence, one has all the information one needs on the trajectory for $\boldsymbol{\alpha}$. Supplying then the values of m_t, m_b, m_τ from experiment, as listed in Table 1, and some assumed values for m_{ν_3} (the "Dirac mass" of the heaviest neutrino ν_3) and the theta-angle θ_{CP} (from the instanton term in the QCD action), one can calculate, using (14), (15), and (17) in the Introduction (plus similar formulae for the other fermion species), the masses $m_c, m_s, m_\mu, m_{\nu_2}, m_u, m_d, m_e, m_{\nu_1}$, as well as the elements of the mixing matrices (CKM for quarks and PMNS for leptons).

All in all, then, there are in the scheme 7 adjustable parameters, namely $a, c, k, R_I, \theta_I, m_{\nu_3}, \theta_{CP}$, of which the last 2 double also as part of the physics

output. From these, one calculates the 8 lower generation masses, 4 independent numbers from the CKM matrix and 3 from the PMNS (thus disregarding an unknown δ_{CP} for leptons, assumed here to be 0), i.e., altogether 17 physical quantities (including m_{ν_3}, θ_{CP}) which are all regarded as independent parameters in the usual formulation of the standard model. In other words, if, by adjusting the 7 parameters, one can calculate all these 17 quantities to agree with experiment, one would have shown that these 17 independent parameters in the standard model can all be replaced by 7 in the FSM.[6]

However, some of these 17 quantities have not yet been measured in, or inferred from, experiment. These include θ_{CP} from QCD, and the Dirac masses m_{ν_i} of the 3 neutrinos (unless one specifies a see-saw mechanism). Further, because of confinement, one can infer from experiment only m_u and m_d when run by QCD to the GeV scale, but not their values at their own mass scales as are needed here. However, the ratio m_u/m_d should remain constant under QCD running. This leaves then, in principle, only 12 of the original 17 quantities to be fitted. However, in practice, we have to fit more, for although there are in theory, because of unitarity, only 4 independent parameters in the CKM matrix, the requirement of only 4 of the elements $|V_{rs}|$ to be within experimental errors is no guarantee that the other 5 will be within errors too, the unitarity conditions being quadratic and some of the elements being much smaller than the others. For this reason, we have to take into account in our fit all the 9 elements of $|V_{rs}|$ together with the Jarlskog invariant J [15]. (The same remarks apply also to the PMNS matrix, but here since only 3 mixing angles have been measured experimentally, there is no other quantity to fit.) This then increases the total number of measured quantities to 18, which are to be fitted by adjusting our 7 parameters.

We shall proceed in the following manner, which we think will give a more transparent test of the FSM scheme than an immediate overall fit to all the 18 listed quantities. We shall first select a subset of the listed quantities, the experimental values of which we shall supply as input so as to determine, by fitting them, the values of the 7 adjustable parameters. Then with the values for the 7 parameters so determined, we shall calculate via FSM the values of the remaining quantities, which can now be taken as predictions of the model to be tested against data, and if they agree, we have a direct test

[6]By the standard model here, we mean that in which the now established fact, that neutrinos have masses and oscillate, is incorporated. This means it will have to carry the Dirac masses of the neutrinos also as parameters. Further, we count θ_{CP} also as a parameter of the standard model although it is often arbitrarily put to zero.

of the FSM against experiment.

We have selected the target quantities to be fitted according to the following criteria:

- that they are sufficient to determine the 7 parameters adequately,
- that they have been measured in experiment to reasonable accuracy,
- that they are sufficiently sensitive to the values of the parameters,
- that they are strategically placed in $t = \ln \mu^2$ over the interesting range,

and we end up with the following choice: the masses m_c, m_μ, m_e and the elements $|V_{us}|, |V_{ub}|$ of the CKM matrix for quarks plus the element $|U_{e3}|$ of the PMNS matrix for leptons (or $\sin^2 2\theta_{13}$), altogether 6 quantities the measured values of which as quoted in the PDG are shown in the second column of the first section of Table 2. That we happen to need only these 6 quantities to fix our 7 parameters is because of the particular way we have chosen to fit the Cabibbo angle, to be explained in the following paragraph, which involves already by itself the choice of 2 of these parameters.

To fit these 6 quantities with the 7 adjustable parameters is then our first task. We choose to do so by trial and error, adjusting judiciously the parameters by hand until we get what we consider a decent fit. We find this much more instructive as to how the fit occurs than by, for example, just mechanically minimizing χ^2, as it is more traditional perhaps to do. In any case, for the present problem, minimising χ^2 would be impracticable without introducing some arbitrary weighting of the data on the 6 quantities to be fitted, given the great disparity in accuracy to which they have been measured in experiment, from order 10^{-8} for the masses of μ and e to merely about 10 percent for $\sin^2 2\theta_{13}$.

Besides, in our trial and error fit, we are guided by experience gathered in previous phenomenological fits to more or less the same data [21], so that we know beforehand which of the 7 parameters is likely to affect which of the 6 targeted quantities most, even though each of the 7 will of course affect all the quantities concerned to some extent. First, as already mentioned in (A) at the beginning of this section, the large value of the Cabibbo angle $|V_{us}|$ requires that the curve Γ traced out by the rotating vector $\boldsymbol{\alpha}$ to have quite sizeable geodesic curvature κ_g around the scale where the Cabibbo angle is measured. This means by Figure 1 that we should choose for a a

smallish magnitude. However, a should not be chosen too small; otherwise the geodesic curvature will be too concentrated all at one point not to leave enough elsewhere to give, for example, a sizeable value also for the solar neutrino angle θ_{13}. A comparison of κ_g to previous fits [21] suggests that a value of $|a| \sim 0.1$ would be about right. Further, to get the maximum benefit of κ_g for the Cabibbo angle, one would put t and b at scales fairly close to the maximum of κ_g on Γ, which means in practice the parameter θ_I also fairly close to that same maximum. Hence roughly, this takes care of already 2 of the 7 parameters.

Next, we turn to the masses m_c, m_μ, m_e. In the rotation picture, as already noted, these are all consequences of rotation and would increase with rotation speed, which is in turn governed by the Yukawa coupling strength ρ_S or c. Hence to fit the overall sizes of the masses, we can adjust the value of c. The relative size of m_c and m_μ, on the other hand, is much conditioned by the proximity of the fixed point at $\mu = \infty$ and $R = 0$, as is explained in (B) at the beginning of this section. Hence, to fit the ratio m_μ/m_c to data, one can adjust the initial value R_I of R. Finally, to fit the value of m_e/m_μ, one can adjust the fudge parameter k which affects most the speed at low scales.

The rotation speed, of course, affects also the overall size of the 2 mixing angles $|V_{us}|$ and $|V_{ub}|$, but not by much their relative sizes. These can be adjusted by adjusting the parameter θ_{CP}, the theta-angle from the instanton term in the QCD Lagrangian which in FSM, we recall, is related to the Kobayashi-Maskawa phase in the CKM matrix.

And with this, we have control now on 6 of the adjustable parameters, namely $a, c, R_I, \theta_I, \theta_{CP}, k$, leaving on our list only the Dirac mass of the heaviest neutrino m_{ν_3} which affects only quantities involving neutrinos. Hence, forgetting those for the moment, we have a good idea how to adjust these 6 parameters to fit the 5 chosen quantities not involving neutrinos, namely $m_c, m_\mu, m_e, |V_{us}|, |V_{ub}|$, and after a few tries, it is not hard to end up with a decent fit. Then, having got this, it is relatively easy to vary m_{ν_3} until we have a fit for $\sin^2 2\theta_{13}$ also. Our best result is shown in the third column of the first section of Table 2, which has been obtained for the following values of our 7 parameters:

$$a = -0.1, \quad c = 0.12, \quad \theta_{CP} = 1.78, \quad k = 2.05,$$

$$R_I = 0.01, \quad \theta_I = -1.33, \quad m_{\nu_3} = 29.5 \text{ MeV}, \tag{51}$$

where the two integration constants (initial values) R_I and θ_I have been taken at $\mu = 250$ GeV for convenience.[7] One notes in Table 2 that the 4 quantities $m_c, |V_{us}|, |V_{ub}|, \sin^2 2\theta_{13}$ have all been fitted to within present experimental errors, while m_μ and m_e, the experimental errors for which are so small as to be inappropriate for us to chase, have been fitted to, respectively, 0.2 and 0.4 percent. This is more than enough accuracy for our present purpose.

Note that the functional form for the trajectory for $\boldsymbol{\alpha}$ (i.e., both the shape of the curve Γ it traces out on the unit sphere and the variable speed at which it moves along that curve) having already been prescribed, it is not at all obvious that the 6 targeted quantities can be so fitted with the given 7 parameters. That it can indeed be done to the accuracy seen in Table 2 constitutes already a quite nontrivial test.

The real test for the model, however, arises when the fitted values of the parameters in (51) are used to evaluate the 12 other measured quantities which have not been selected by us as targets for fitting. As far as the standard model is concerned, 6 of these are independent of one another and of the 6 quantities which have been fitted, and so, in principle, can have any value they choose, and if the RGE derived from the FSM can reproduce their values, even approximately, it would be a much welcome success. They cannot be claimed as predictions, for their empirical values are known, and we can and did monitor their theoretical values produced by our scheme as we vary our parameters to perform the fit. But there is little we can do to influence their values since the parameters have to be chosen to fit the 6 selected quantities as we have done above. In other words, once the above fitting procedure is adopted, the values of the output quantities are entirely at the mercy of the rotation equations and out of our control altogether. Their agreement or otherwise with experiment would thus be a genuine test for the FSM's validity.

The output quantities of our fit with (51) are shown in the third column and compared with their present experimental values in the second column of the second section of Table 2. We note that of the 12 numbers shown, 6 are within experimental error or 1σ or else (m_μ, m_e) within 0.5 percent of the accurate measured values, while 2 are within $\sim 1.5\sigma$. Of the remaining 4, 1 (m_s) can only be roughly compared with experiment, because of QCD

[7] The negative value we quote for the polar angle θ_I may seem surprising, but it is actually no more than a convention (see Appendix) adopted for convenience in our numerical calculation.

	Expt (June 2014)	FSM Calc	Agree to	Control Calc
INPUT				
m_c	1.275 ± 0.025 GeV	1.275 GeV	$< 1\sigma$	1.2755 GeV
m_μ	0.10566 GeV	0.1054 GeV	0.2%	0.1056 GeV
m_e	0.511 MeV	0.513 MeV	0.4%	0.518 MeV
$\|V_{us}\|$	0.22534 ± 0.00065	0.22493	$< 1\sigma$	0.22468
$\|V_{ub}\|$	$0.00351^{+0.00015}_{-0.00014}$	0.00346	$< 1\sigma$	0.00346
$\sin^2 2\theta_{13}$	0.095 ± 0.010	0.101	$< 1\sigma$	0.102
OUTPUT				
m_s	0.095 ± 0.005 GeV (at 2 GeV)	0.169 GeV (at m_s)	QCD running	0.170 GeV
m_u/m_d	0.38—0.58	0.56	$< 1\sigma$	0.56
$\|V_{ud}\|$	0.97427 ± 0.00015	0.97437	$< 1\sigma$	0.97443
$\|V_{cs}\|$	0.97344 ± 0.00016	0.97350	$< 1\sigma$	0.97356
$\|V_{tb}\|$	$0.999146^{+0.000021}_{-0.000046}$	0.99907	1.65σ	0.999075
$\|V_{cd}\|$	0.22520 ± 0.00065	0.22462	$< 1\sigma$	0.22437
$\|V_{cb}\|$	$0.0412^{+0.0011}_{-0.0005}$	0.0429	1.55σ	0.0429
$\|V_{ts}\|$	$0.0404^{+0.0011}_{-0.0004}$	0.0413	$< 1\sigma$	0.0412
$\|V_{td}\|$	$0.00867^{+0.00029}_{-0.00031}$	0.01223	41 %	0.01221
$\|J\|$	$\left(2.96^{+0,20}_{-0.16}\right) \times 10^{-5}$	2.35×10^{-5}	20 %	2.34×10^{-5}
$\sin^2 2\theta_{12}$	0.857 ± 0.024	0.841	$< 1\sigma$	0.840
$\sin^2 2\theta_{23}$	> 0.95	0.89	$> 6\%$	0.89

Table 2: Calculated fermion masses and mixing parameters compared with experiment

running as already explained, and it does so compare quite reasonably. The other 3: $|V_{td}|, J, \sin^2 2\theta_{23}$, are all outside the stringent experimental errors, but still not outrageously so. Besides, $|V_{td}|$ and J both being small and therefore delicate to reproduce, obtaining them with the right order of magnitude as they are here is already no mean task. We note in particular the interesting output for m_u/m_d which not only confirms the elusive but crucial empirical fact that $m_u < m_d$ but even gives the ratio within the present PDG quoted error. That the ratio should agree numerically may perhaps be a little fortuitous, but that m_u should come out smaller than m_d appears generic to the FSM, which is an important point to which we shall shortly return.

To us, this is about as good a result as one can hope to get with the approximate RGE (49), (47) and (48) derived merely at 1-loop and especially with a fudge on k, replacing that function of scale by a constant. Indeed, we do not mean, by carrying as many significant figures as we do in the numbers cited in Table 2, that we believe the set-up, as it is, is actually correct to this sort of accuracy. We do so merely as a test, to see to what sort of accuracy that an FSM fit is capable of. Besides, with our trial and error approach to fitting, we cannot claim that the present fit is the best fit even in the vicinity in parameter space of the present one. There may also be even better fits in other parts of the parameter space, e.g. when $R < 0$, that we have not yet sufficiently explored. But one can reasonably claim, we think, that this fit has demonstrated that the FSM is capable of giving a very sensible description of the mass and mixing data, as one has hoped.

To check our numerical result, a second calculation is done by another program in another language using the same parameters (51). This gives the result shown in the last column of Table 2. Besides confirming the result of the earlier calculation displayed in the third column, it provides an estimate for the numerical accuracy of our results, which otherwise would not be easy to obtain. Some numerical details of the calculation is given in the Appendix so that interested readers can do spot checks on our numbers if they so wish.

The fit gives in addition the following values for the 5 other standard model parameters which, not being measured, cannot as yet be checked against experiment:

$$\theta_{CP} = 1.78, \quad m_u(\mu = m_u) = 0.22 \text{ MeV } [\text{or } m_d(\mu = m_d) = 0.39 \text{ MeV}],$$
$$m_{\nu_3} = 29.5 \text{ MeV}, \quad m_{\nu_2} = 16.8 \text{ MeV}, \quad m_{\nu_1} = 1.4 \text{ MeV}. \tag{52}$$

The curve traced out by the rotating $\boldsymbol{\alpha}$ for the value of a listed in (51) is

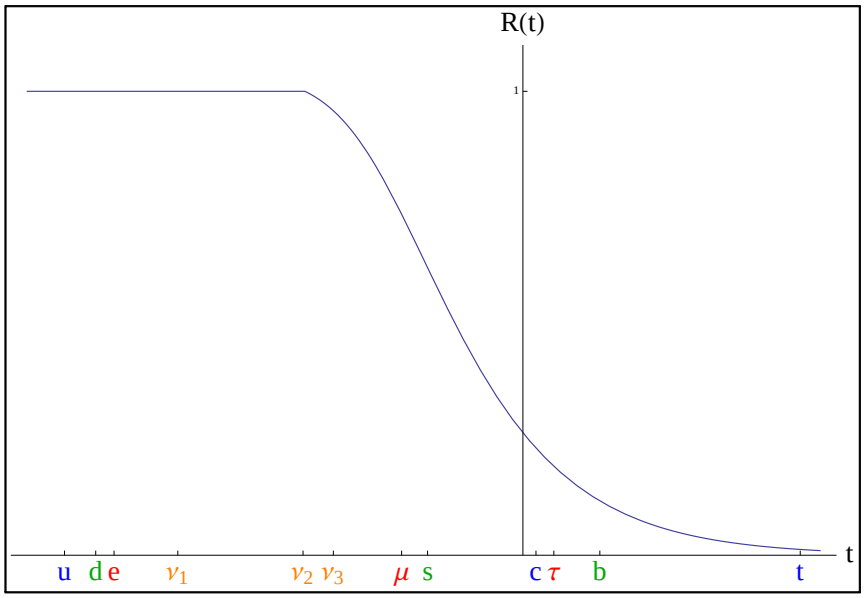

Figure 2: Solution of the RGE (47) for R as a function of $t = \log \mu^2$, where μ is the scale in GeV, obtained with parameters given as in (51).

shown already as the curve in orange in Figure 1. The solutions of (47) and (48) for R and θ as functions of the scale μ are shown in Figures 2 and 3. The actual trajectory for $\boldsymbol{\alpha}$ on the unit sphere is given in Figures 4, 5 and 6, and from these, one gets a clear visual picture of how, qualitatively, most of the results in Table 2 come about.

From the fixed point at $R = 0$ and $\mu = \infty$, one sees from Figures 3 and 6 that rotation starts slowly, but accelerates for decreasing μ as it is expected that it should. As explained in (B) above, this would account, by the leakage mechanism, for the experimental fact that $m_c/m_t < m_s/m_b < m_\mu/m_\tau$. Comparing Figures 4 and 6, one sees that in the region where these 6 fermions are placed, rotation is still rather slow, so that to get a sizeable Cabibbo angle, Γ would need to have large geodesic curvature in this region, and it is seen that it does, which is occasioned by us choosing in (51) a small magnitude for a (0.1) and a value for θ_I (-1.33) close to the maximum for the geodesic curvature. As the scale lowers further, acceleration is seen to continue with, in fact, the rotation speed becoming very large around $t \sim -3.5$ or $\mu \sim 17$ MeV. Now such a rapid rise cannot be ascribed to the said fixed point at $R = 0$ alone, but arises from another source in the RGE,

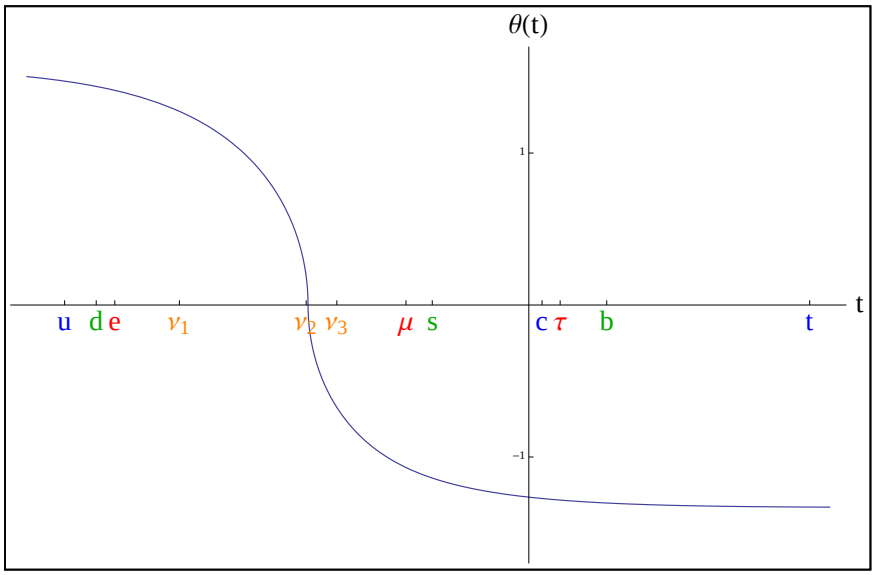

Figure 3: Solution of the RGE (48) θ as a function of $t = \log \mu^2$, where μ is the scale in GeV, obtained with parameters given as in (51).

namely from the denominator D in (48) as explained in (B) above. One notes from Figures 2 and 3 that, at these low values of μ, R is already very near its asymptotic value 1, so that the situation is very close to that described in (B) above. It gives thus fast rotation at the sort of scales just where, for example, m_{ν_3} is placed, and where mixing angles of leptons are evaluated. It follows then, as already explained in (B), that mixing angles for leptons are generally larger than those for quarks, even though the geodesic curvature there at the mass scales for leptons is already far from maximum.

One sees therefore that from the qualitative features of the trajectory for $\boldsymbol{\alpha}$, one can already envisage an outline for the mass and mixing patterns vaguely similar to what is experimentally observed. But that a detailed fit of the data to the accuracy actually achieved in Table 2 is surprising and cannot at first be anticipated.

As the scale lowers further still, the effect of both the fixed point at $R = 0$ and the denominator D dies down and rotation will slow down. But there is yet another twist in the tale from the tail of Γ with interesting consequences. One is now at scales of order MeV where masses of the lowest generation quarks occur. Now according to (15) above, the mass of the u and d quarks

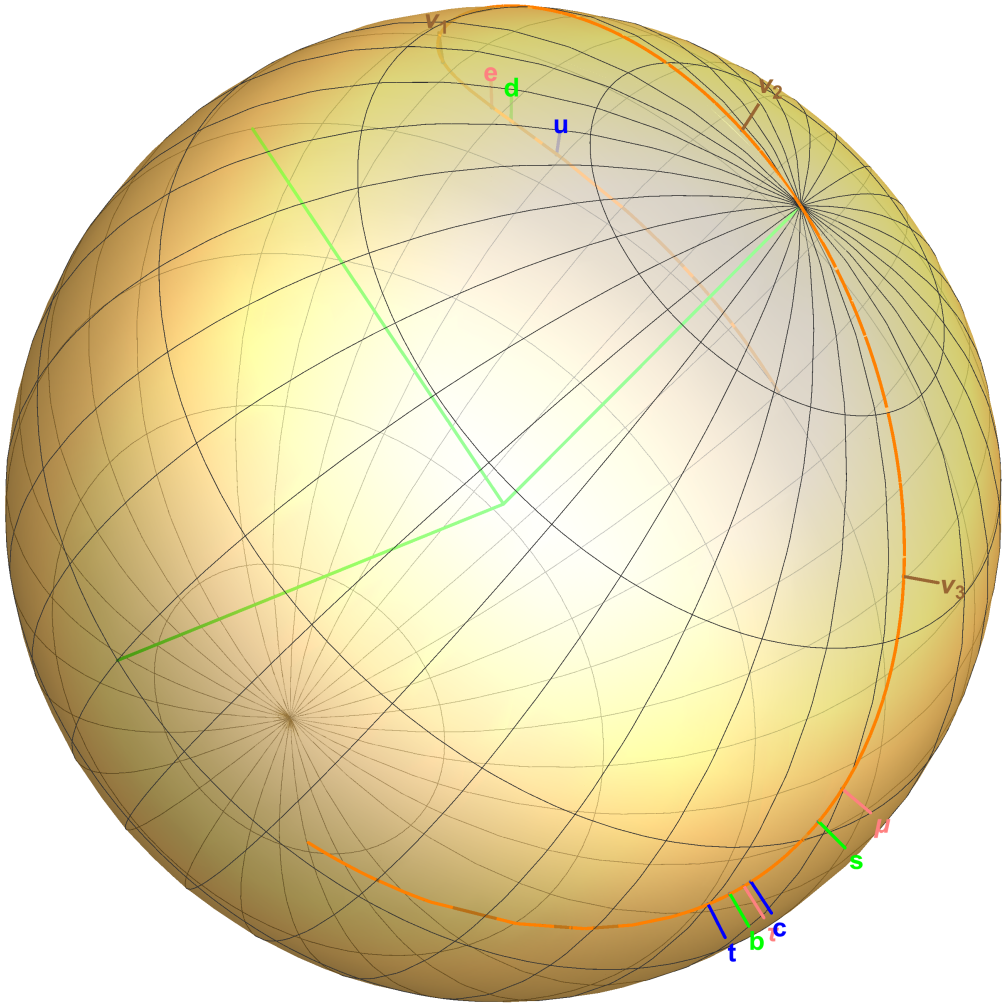

Figure 4: The trajectory for $\boldsymbol{\alpha}$ on the unit sphere in generation space obtained from the parameter values given in (51), showing the locations on the trajectory where the various quarks and leptons are placed: high scales in front.

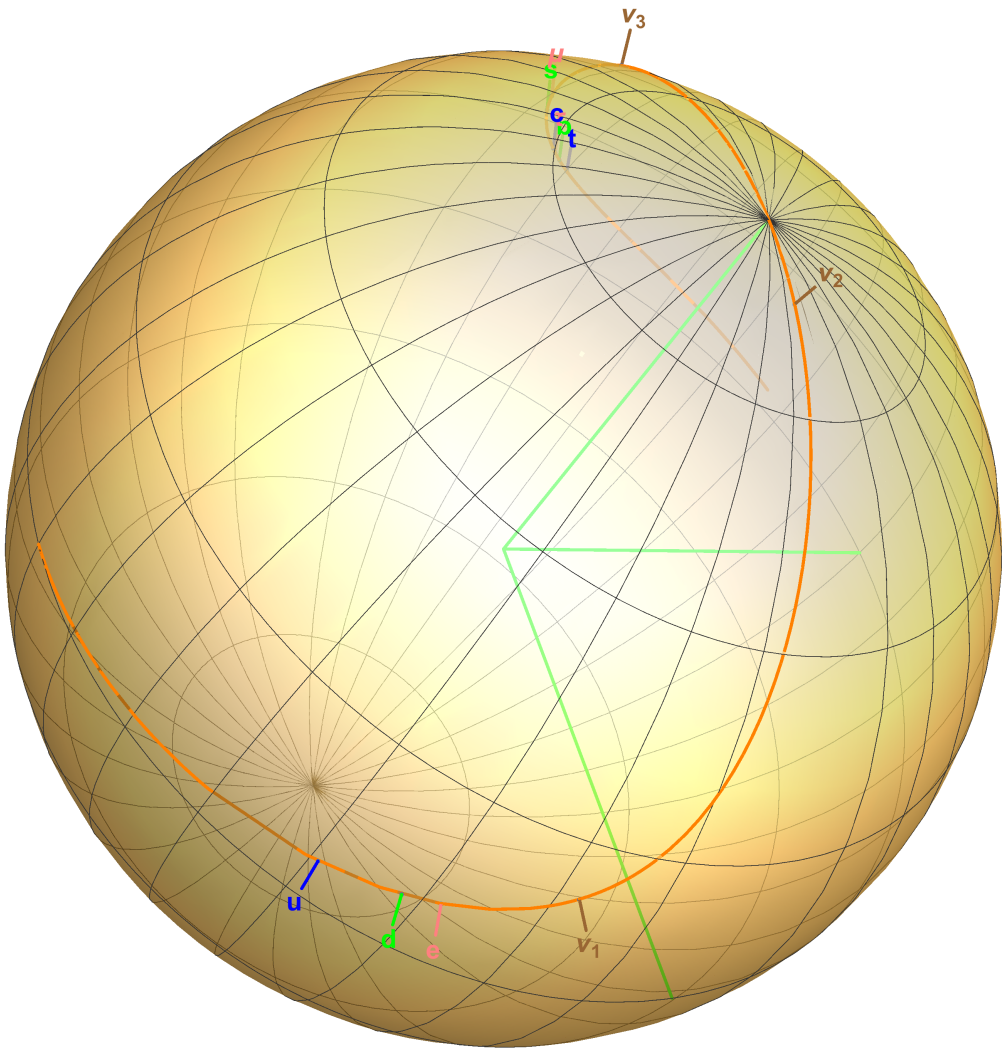

Figure 5: The trajectory for $\boldsymbol{\alpha}$ on the unit sphere in generation space obtained from the parameter values given in (51), showing the locations on the trajectory where the various quarks and leptons are placed: low scales in front.

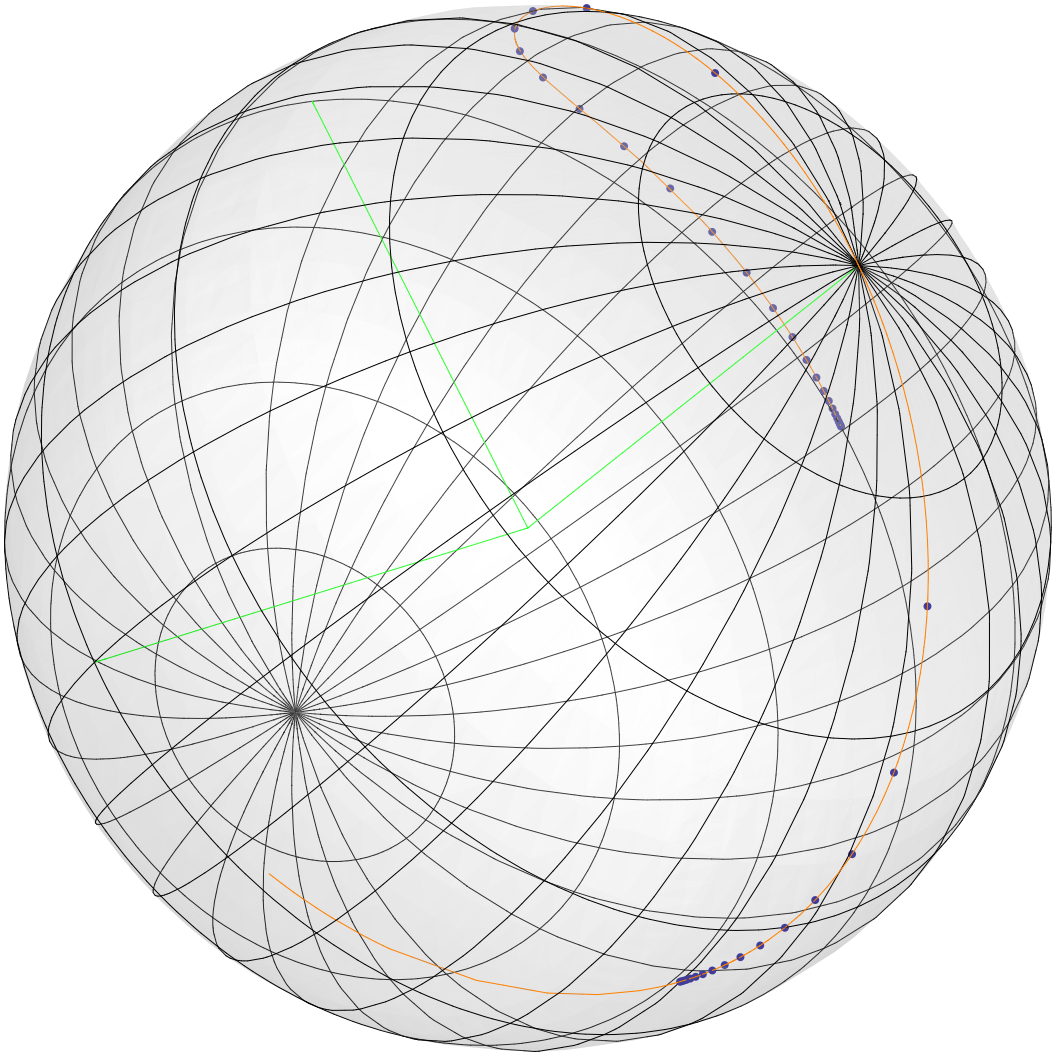

Figure 6: The trajectory for $\boldsymbol{\alpha}$ on the unit sphere in generation space obtained from the parameter values given in (51), showing the distance on Γ travelled by $\boldsymbol{\alpha}$ for every half-decade decrease in scale μ. The high scale region is shown in front.

in FSM are to be given respectively by solution of the equations:

$$|\langle \mathbf{u}|\boldsymbol{\alpha}(\mu)\rangle|^2 = \mu, \quad |\langle \mathbf{d}|\boldsymbol{\alpha}(\mu)\rangle|^2 = \mu, \tag{53}$$

where $\mathbf{u}$ the state vector of u is of course orthogonal to $\mathbf{t}$ and $\mathbf{c}$, the state vectors of t and c. Similarly for the triad $\mathbf{b}, \mathbf{s}, \mathbf{d}$. The masses of u (d) being only of order MeV, this means that one has an approximate solution for $m_u(m_d)$ whenever the vector $\boldsymbol{\alpha}$ crosses the **tc**-plane (**bs**-plane). Given the ordering of the masses of t, b and that, as noted before, $m_c/m_t < m_s/m_b$, the picture is as shown in Figure 7. It is thus clear that in the MeV region where the geodesic curvature has the opposite sign to that in the high scale region, the vector $\boldsymbol{\alpha}$ must cross the **bs**-plane before (i.e. at a higher scale than) the **tc**-plane. In other words, m_d must be larger than m_u, as experiment wants.[8]

That $m_u < m_d$ is of course a crucial empirical fact, without which the proton would be unstable and we ourselves would not exist. It is, however, surprising from the theoretical point of view, given that in the two heavier generations, the ordering of masses is the other way round, namely $m_t \gg m_b, m_c \gg m_s$. This is particularly so from the point of view of rotating mass matrix (R2M2) schemes [8], of which the FSM is one, in which masses for the lower generations are supposed to come from "leakage" due to rotation from the heavier states; so why should the up states leak so much less to the u than the down states to the d? It was a question we kept asking since we first began with the rotation mechanism, but failed to answer. Intriguingly, it is now seen to turn upon the fact that the geodesic curvature κ_g of the curve Γ changes sign when it passes through the pole $\theta = 0$. The sign-change occurs whatever is the value of the integration constant a upon which Γ depends. And this shape of Γ in the FSM, we recall, is the consequence of a symmetry in the framon potential V in (4), which is itself a consequence of the intrinsic symmetry of the framed theory. It is thus a property intrinsic and peculiar to the FSM, which is hard to foretell or imagine otherwise. Phenomenologically, extrapolating from the higher scale region where most of the data lie, one would tend, as we did [21], to assume the same sign for κ_g throughout, and come to the wrong conclusion.

As already mentioned, no estimate of the physical masses of neutrinos can be made in the above FSM fit without additional assumptions on the see-saw mechanism. If we now assume the simplest, namely that there is

[8] One has chosen here the second (lower) solution for u and d as one did also for e in (2). For more elucidation on this point, see Appendix.

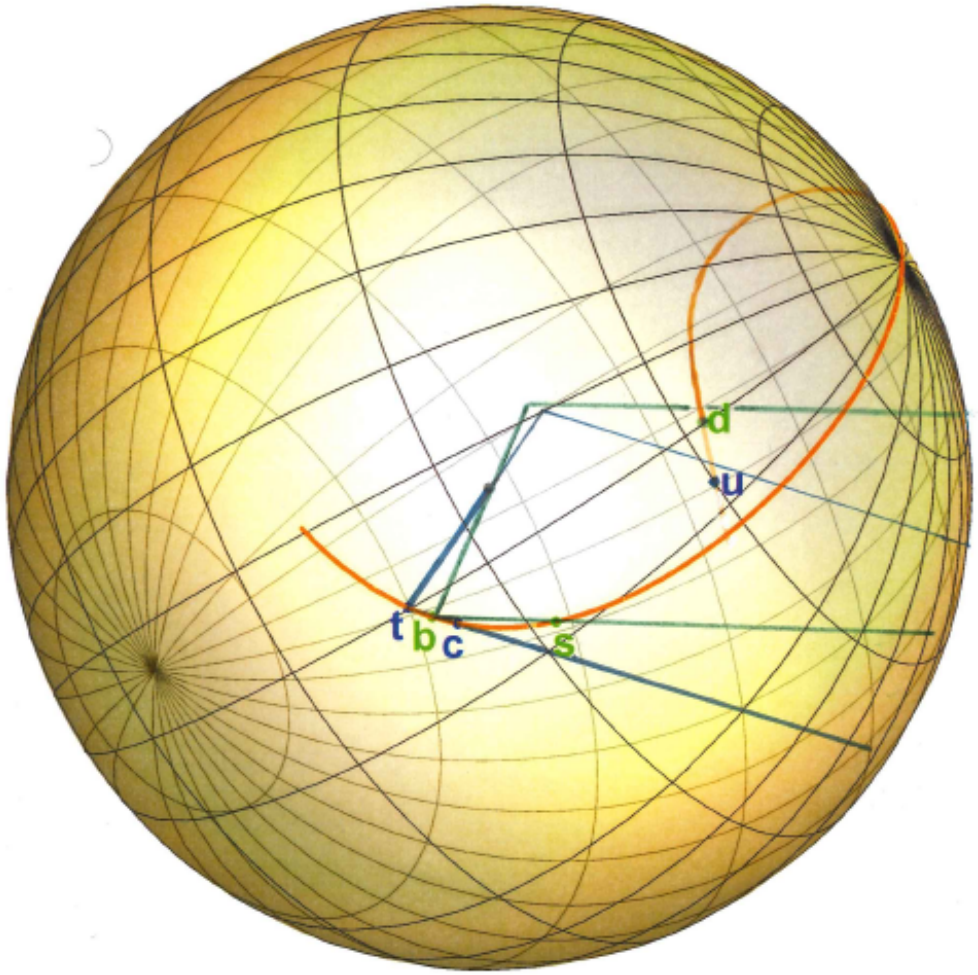

Figure 7: Figure illustrating the reason why $m_u < m_d$ in Table 2.

only one right-handed neutrino with mass m_R, then the physical neutrino masses are given in terms of the Dirac masses just as $m^{\rm ph}_{\nu_i} = m^2_{\nu_i}/m_R$ [12]. Hence, choosing $m_R \sim 17430$ TeV to fit the experimental value:

$$(m^{\rm ph}_{\nu_3})^2 - (m^{\rm ph}_{\nu_2})^2 = (2.23^{+0.12}_{-0.08}) \times 10^{-3}\ {\rm eV}^2, \tag{54}$$

one has:

$$m^{\rm ph}_{\nu_3} \sim 0.050\ eV, \quad m^{\rm ph}_{\nu_2} \sim 0.016\ {\rm eV}, \quad m^{\rm ph}_{\nu_1} \sim 0.0001\ {\rm eV}. \tag{55}$$

Apart from satisfying the, at present, very loose experimental bounds on these individual mass values, this gives:

$$(m^{\rm ph}_{\nu_2})^2 - (m^{\rm ph}_{\nu_1})^2 \sim 2.6 \times 10^{-4}\ {\rm eV}^2, \tag{56}$$

which is at least of the same order as, though some 3 times bigger than, the experimental value of:

$$(m^{\rm ph}_{\nu_2})^2 - (m^{\rm ph}_{\nu_1})^2 = (7.5 \pm 0.20) \times 10^{-5}\ {\rm eV}^2. \tag{57}$$

The discrepancy, however, is not as bad as it looks, for this quantity depends on the rotation angle raised to the 8th power, and the present discrepancy corresponds to an error of only 17 percent in the rotation angle, which is not exorbitant in the scale region where the ν_2 finds itself in the fit, namely near $\theta = 0$ where, as seen in Figures 3 and 6 the rotation speed is very large.

5 Remarks

[I] The RGE for the rotation of $\boldsymbol{\alpha}$ derived in Section 3 from renormalization by framon loops was applied down to scales as low as the electron mass $\sim$ MeV. This presupposes that there are framons of such low masses to drive rotation at such scales, for it is generally believed that particles of high mass cannot give renormalization effects at scales much lower than their own mass scales [23]. One would like to check, therefore, whether in the FSM scheme there are indeed framons of such low masses.

Expanding the framon potential (4) to second order in fluctuations about its vev, one obtains to tree-level the mass matrix of the framon-Higgs states

(i.e., the standard Higgs h_W together with the 9 strong Higgs states H_K) as:

$$M_H = \begin{pmatrix} 4\lambda_W\zeta_W^2 & 2\zeta_W\zeta_S(\nu_1-\nu_2)\sqrt{\frac{1+2R}{3}} & 2\sqrt{2}\zeta_W\zeta_S\nu_1\sqrt{\frac{1-R}{3}} & 0 \\ * & 4(\kappa_S+\lambda_S)\zeta_S^2\left(\frac{1+2R}{3}\right) & 4\sqrt{2}\lambda_S\zeta_S^2\frac{\sqrt{(1+2R)(1-R)}}{3} & 0 \\ * & * & 4(\kappa_S+2\lambda_S)\zeta_S^2\left(\frac{1-R}{3}\right) & 0 \\ 0 & 0 & 0 & D \end{pmatrix} \tag{58}$$

where

$$D = \kappa_S\zeta_S^2 \begin{pmatrix} 4(\frac{1-R}{3}) & 0 & 0 & 0 & 0 & 0 & 0 \\ 0 & 4(\frac{1-R}{3}) & 0 & 0 & 0 & 0 & 0 \\ 0 & 0 & 4(\frac{1-R}{3}) & 0 & 0 & 0 & 0 \\ 0 & 0 & 0 & 2(\frac{2+R}{3}) & 0 & 0 & 0 \\ 0 & 0 & 0 & 0 & 2(\frac{2+R}{3}) & 0 & 0 \\ 0 & 0 & 0 & 0 & 0 & 2(\frac{2+R}{3}) & 0 \\ 0 & 0 & 0 & 0 & 0 & 0 & 2(\frac{2+R}{3}) \end{pmatrix} \tag{59}$$

and where an $*$ denotes the corresponding symmetric entry. The rows and columns of this matrix are labelled by the Higgs states listed in (12) except for the third and fourth row (column) which correspond respectively to $H_\pm = (H_2 \pm H_3)/\sqrt{2}$.

We note that apart from the h_W, which of course stands by itself, the others, H_K, fall into 3 categories, with masses proportional respectively to $\sqrt{1+2R}, \sqrt{1-R}, \sqrt{2+R}$. A few of them are mixed in the present basis, but most of them are already diagonal. Among the 9 H_K's, there are 4 with masses proportional $\sqrt{1-R}$. Now recall from Figures 2 and 3 the behaviour of R as the scale μ decreases from ∞. By the scale of around 20 MeV when θ crosses 0, $R \to 1$ so that the states H_K with masses proportional to $\sqrt{1-R}$ approach zero also. In other words, in the present fit, there will indeed always be H_K's with low enough masses to drive rotation down to the low scales one wants.

The other H_K states with masses proportional to $\sqrt{1+2R}$ and $\sqrt{2+R}$, however, will remain of order ζ_S, whose magnitude one has at present no estimate for, but presumably $>$ MeV. In that case, they cannot, according to the above, contribute to driving the rotation at very low scales, so that the RGE derived in Section 3 by summing over all H_K should in principle be modified. Unfortunately, to take account of the suppression of these states with its many inherent uncertainties, would introduce more freedom and

parameters than can be handled at present. These modifications, however, will likely affect only the rotation speed of $\boldsymbol{\alpha}$ in (47) and (48), not the shape of Γ in (49) which comes from the residual $\widetilde{su(2)}$ symmetry mentioned in (A).

[II] To help gauge the significance of the fit given in Section 4, one could compare it with other fits of the same data, but we are not aware of other fits in the literature attempting, all at one go, a similar fit to the mass and mixing data for both quarks and leptons, excepting some of our own. Previous to the present, our most successful fit to these data was the phenomenological fit of [21], to which one can thus make comparison.

Such a comparison, however, would be grossly unfair, given that in [21] one is allowed to choose freely both the shape and speed functions for the rotation trajectory so as to fit the data, whereas here, in the present fit, both these functions are constrained by the RGE derived from the FSM. Nevertheless, the comparison in quality of the resulting fits is very much in favour of the present one. For scales μ above 20 MeV, the fits are similar in quality, as can be seen by comparing Table 2 to corresponding results in [21], the small differences being due just to differences in emphasis on which bits of data one chooses to fit better than others. For scales below 20 MeV, on the other hand, the present fit wins on 3 significant points:

- m_e is on the dot,
- $m_u < m_d$,
- the trajectory has finite length, thus avoiding there being too many solutions for the the lowest generation,

none of which is matched by [21]. Although the first result can be ascribed to an extra parameter in the present fit (7 here instead of 6 in [21]), the other 2 results are "predictions" of the FSM, which was not, and could not have been, anticipated in the purely phenomenological approach taken in [21].

[III] Besides fitting existing data as is done in this paper, one could try to test the FSM by predicting some new phenomena to be tested by experiment. However, for these, one will need first to develop logically the rules in FSM for calculating quantities such as decay widths and scattering amplitudes and so on, i.e., beyond the single particle quantities like masses and mixing

parameters considered in this paper. To develop such rules will take time, given the new concept of a rotating mass matrix involved.

In the absence of standard rules to perform actual calculations, one can at present only make surmises, but some of these might already be quite exciting. For instance, an examination of Higgs decays in [8, 22] led to the tentative conclusion that there may be, in these decays, sizeable flavour-violating modes, based on arguments which ran briefly as follows. Recall first the Yukawa coupling in (13) above from which the quark and lepton mass matrix (1) was derived. From this it would seem to follow that the coupling of the Higgs boson would carry with it the same factor $\boldsymbol{\alpha}\boldsymbol{\alpha}^\dagger$ as did the mass matrix. Since $\boldsymbol{\alpha}$ is supposed to rotate with scale, one has to specify at which scale to take this $\boldsymbol{\alpha}$, and we suggested $\mu = m_H$. Sandwiching this now between, say, a lepton state ℓ on one side and another lepton state ℓ' on the other, one would obtain an amplitude for $H \to \bar{\ell}\ell'$ proportional to $\langle\ell|\boldsymbol{\alpha}\rangle\langle\boldsymbol{\alpha}|\ell'\rangle$, or a decay width proportional to $|\langle\boldsymbol{\alpha}|\ell\rangle|^2|\langle\boldsymbol{\alpha}|\ell'\rangle|^2$. which has no identifiable reason to be zero for $\ell \neq \ell'$. Hence flavour violation as anticipated.

Given the above fit reported in Section 4, $\boldsymbol{\alpha}$ is known at $\mu = m_H$, now measured experimentally at 126 GeV, and since the state vectors $\boldsymbol{\tau}$ and $\boldsymbol{\mu}$ are also known, the actual width of the flavour-violating mode $H \to \bar{\tau}\mu$, say, relative to $H \to \bar{\tau}\tau$ can be estimated:

$$\frac{\Gamma(H \to \bar{\tau}\mu)}{\Gamma(H \to \bar{\tau}\tau)} = \frac{|\langle\boldsymbol{\alpha}|\mu\rangle|^2}{|\langle\boldsymbol{\alpha}|\tau\rangle|^2} \sim 2 \times 10^{-4}. \tag{60}$$

This is still some 2 orders below the bound given recently by CMS for this mode, but in future might be an interesting point to watch.[9]

[IV] There is yet a wide area of phenomenology opened up by the framing hypothesis waiting to be explored. The new ingredients added by framing to the standard model are the framons, of which the weak component is identified as the standard Higgs field. This leaves the strong framons as the main new ingredients, and it is these that give rise, according to the RGE derived in Section 3, to the rotation of the mass matrix, and hence to the fermion mass hierarchy and mixing phenomenon, the effects which gave the

[9]Intriguingly, CMS [24] actually saw a slight excess above background for this mode, but only at the 2σ level. Besides, with a best-fit BR of about 0.009, this excess would in any case be much too large to be explained by the above effect.

first incentive for the framing hypothesis. But now, given these new framon degrees of freedom, would it not also lead to new physical phenomena that one has not anticipated? And may not these afford even better and more direct tests of the framing hypothesis than the rather round-about test that we have here performed? Would it not be more direct experimentally to try looking for these strong framons themselves?

The strong framons, however, are coloured, and so are confined by colour $su(3)$. Hence, they will not exist as free particles in space but have to be looked for inside hadronic matter. There, they can contribute to renormalization effects, for example, as gluons do, to the running of the strong coupling g. But here, being scalar bosons, they contribute very little to the running speed, which is unlikely to be noticeable for some time [25]. There may, of course, be other effects in which the renormalization by strong framon loops is more prominent. The rotation of the fermion mass matrix investigated above is one such example, but we do not yet know of others.

One might, perhaps, expect to see framons hadronizing, as quarks and gluons do, and appearing as jets in collisions with high impact. But this seems to us unlikely, for strong framons in (4) have $\mu_S > 0$, which means that they are "ghosts" with imaginary masses, and hence, unlike quarks and gluons, cannot propagate in hadronic matter.

However, a strong framon can form bound states with a strong antiframon by colour confinement, thus $\bar{\boldsymbol{\phi}}^{\bar{a}}\boldsymbol{\phi}^{\tilde{b}}$, which are then the strong Higgs states H_K, the loops of which generate the RGE's in Section 3, and the tree-level mass matrix of which is given in (59) above. These being just hadrons, can propagate freely in space and be detected by experiment in principle. Unfortunately, one does not yet know exactly where to look, because their masses depend on parameters such as ζ_S, κ_S and λ_S for the values of which one has no estimate at present. Suppose these parameters are such that all H_K's have large masses, then, being hadrons, they are likely to have big widths as well, in which case they will be hard to find and might escape detection up until the present. But in that case, it would be hard to understand why they can still drive rotation of the fermion mass matrix down to the scales we want. But, on the other hand, if we accept the conclusion in [I] above that some of the the H_K's have small masses at low scales, low enough to drive rotation to the low scales we want, then they should be observable. But then where are they, and why have they not been seen? There is, intriguingly, an exciting possible solution to this apparent dilemma which we have been

considering recently, but this being rather speculative at present, even if it should work out, would be at variance with the stolid pragmatism intended for the present paper. We shall leave it, we hope, to be presented elsewhere.

Appendix. Some details to facilitate spot checking of numerical results

In solving the equations (47) and (48) numerically by iteration, a technical point is encountered which is worth noting. These equations are given in polar co-ordinates θ, ϕ where by standard convention, $0 < \theta < \pi,\ 0 < \phi < 2\pi$, so that, given the sign in (48), θ will decrease with increasing μ. On reaching the point $\theta = 0$, therefore, and also thereafter when μ increases further, the output θ from iterating the equation (48) must turn negative, just by continuity as befits a solution of differential equations. This may seem disturbing at first sight, but is in fact no more than a renaming of the points further along the trajectory beyond $\theta = 0$ by the unconventional, though equally unambiguous, polar co-ordinates $-\theta, \phi$ instead of the more conventional $\theta, \pi + \phi$. In the equations themselves, however, the θ appearing there is still to be understood in the standard convention so that the output θ will continue to decrease with increasing μ and become more and more negative. One sees then that when thus understood, the solution will just go smoothly over $\theta = 0$, and continue on to the other side. What we actually did, as is natural in FSM, however, was the other way round, i.e., iterate from high to low scale instead. We then found it convenient to adopt the convention that the output θ is negative at high scales, then changes sign to positive when θ crosses 0 into the low μ region. This is the convention adopted in the value for θ_I in (51) and in Figure 3.

For the parameters given in (51), our numerical solution of the RGE gives $\boldsymbol{\alpha}$ at the mass scales of the various quark and lepton states as:

$$\begin{aligned}
\boldsymbol{\alpha}^\dagger(\mu = m_t) &= (-0.89580,\ \ 0.37467,\ \ 0.23909) \\
\boldsymbol{\alpha}^\dagger(\mu = m_b) &= (-0.90212,\ \ 0.34069,\ \ 0.26479) \\
\boldsymbol{\alpha}^\dagger(\mu = m_\tau) &= (-0.90435,\ \ 0.31923,\ \ 0.28329) \\
\boldsymbol{\alpha}^\dagger(\mu = m_{\nu_3}) &= (-0.62012,\ \ 0.07942,\ \ 0.78048) \\
\boldsymbol{\alpha}^\dagger(\mu = m_c) &= (-0.90487,\ \ 0.30860,\ \ 0.29321)
\end{aligned}$$

$$
\begin{aligned}
\boldsymbol{\alpha}^\dagger(\mu = m_s) &= (-0.88316,\ \ 0.21072,\ \ 0.41907) \\
\boldsymbol{\alpha}^\dagger(\mu = m_\mu) &= (-0.85897,\ \ 0.17903,\ \ 0.47971) \\
\boldsymbol{\alpha}^\dagger(\mu = m_{\nu_2}) &= (0.17880,\ \ -0.01812,\ \ 0.98372) \\
\boldsymbol{\alpha}^\dagger(\mu = m_u) &= (0.71377,\ \ -0.69284,\ \ 0.10251) \\
\boldsymbol{\alpha}^\dagger(\mu = m_d) &= (0.80422,\ \ -0.57797,\ \ 0.13847) \\
\boldsymbol{\alpha}^\dagger(\mu = m_e) &= (0.83746,\ \ -0.52272,\ \ 0.15944) \\
\boldsymbol{\alpha}^\dagger(\mu = m_{\nu_1}) &= (0.90360,\ \ -0.33147,\ \ 0.27136)
\end{aligned} \tag{61}
$$

and the state vectors of the various quark and lepton states as:

$$
\begin{aligned}
\mathbf{t}^\dagger &= (-0.89580,\ \ 0.37467,\ \ 0.23909) \\
\mathbf{b}^\dagger &= (-0.90212,\ \ 0.34069,\ \ 0.26479) \\
\boldsymbol{\tau}^\dagger &= (-0.90435,\ \ 0.31923,\ \ 0.28329) \\
\boldsymbol{\nu}_3^\dagger &= (-0.62012,\ \ 0.07942,\ \ 0.78048) \\
\mathbf{c}^\dagger &= (-0.14421,\ \ -0.75386,\ \ 0.64102) \\
\mathbf{s}^\dagger &= (0.00217,\ \ -0.61007,\ \ 0.79235) \\
\boldsymbol{\mu}^\dagger &= (0.07434,\ \ -0.53580,\ \ 0.84107) \\
\boldsymbol{\nu}_2^\dagger &= (0.77494,\ \ -0.09291,\ \ 0.62517) \\
\mathbf{u}^\dagger &= (0.42041,\ \ 0.53974,\ \ 0.72934) \\
\mathbf{d}^\dagger &= (0.43148,\ \ 0.71537,\ \ 0.54961) \\
\mathbf{e}^\dagger &= (0.42028,\ \ 0.78168,\ \ 0.46082) \\
\boldsymbol{\nu}_1^\dagger &= (0.12217,\ \ 0.99250,\ \ -0.00393).
\end{aligned} \tag{62}
$$

The $\boldsymbol{\alpha}$'s in (61) are easily checked to lie on the curve Γ given by (49) but to check that they have indeed the locations on Γ as are given, one will need to solve the RGE's (47) and (48) for the rotation speed. Next, the state vectors for the quarks and leptons given in (62) are also easily checked to be consistent with their definition in (14) (and similar expressions for the other species) in terms of the $\boldsymbol{\alpha}$'s given in (61). From (62) and (61), then, the masses of the various quark and lepton states can be readily calculated by (15). They will be seen to tally with the results given in Table 2 and (52), except for u, and to a less extent for e, where the agreement may not be to the accuracy indicated for a rather trivial technical reason.[10] Further, from (62), the PMNS matrix elements for leptons can be calculated (assuming δ_{CP}

[10]The left-hand side of the equation (15) for m_u being rapidly varying as a function of

to be zero for leptons, as was done in Table 2) just as the inner products of the state vectors, and hence the angles θ_{ij} to be deduced and checked against the given values in Table 2. And finally, given further the following:

$$\sin\omega_U = -0.1019, \quad \sin\omega_D = -0.2506 \tag{63}$$

obtained in our calculation, together with the value given in (52) for θ_{CP}, one can calculate the CKM matrix via (16) and (17) to be checked against Table 2.

The lightest generation fermions, namely u, d, e and ν_1, need some extra clarification. In contrast to the 2 heavier generations, the equations (15) for the masses of these lightest states can have in general multiple solutions[11]. In the present FSM case, there are 3 solutions for u, d, e but only 1 for ν_1, which last therefore needs no further discussion. Of each of u, d, e, one solution is much higher in mass than the other two, and this we discard, since it would be unstable against decay into the lower two. The two remaining solutions are very close in mass, differing only by order 10 keV. As already noted above, around (53), an approximate solution for u occurs whenever $\boldsymbol{\alpha}$ crosses the **tc**-plane, if one neglects some small effects, but when these small effects are taken into account, this solution splits into 2, one placed slightly above and one slightly below the **tc**-plane. We have not understood the reason for this doubling of what appears to be but a single solution. The numbers in Table 2 are for the higher of these two solutions, but since the differences are so small, very similar results would be obtained by focusing instead on the lower, or on the average of the two. Obviously, some further thinking is needed from us to understand why there should be this doubling.

---

m_u in the MeV region, we chose in our numerical fitting program to take, as solution for m_u, the value at which the difference Δ between the left-hand and right-hand sides of (15) changes sign from m_u to $m_u + \delta\mu$. This ensures the accuracy of the solution for m_u to be within the spacing $\delta\mu$, but may not give to a similar accuracy the left-hand side of (15), or $\boldsymbol{\alpha}(m_u)$. However, this is a valid procedure because the accurate value for $\boldsymbol{\alpha}(m_u)$ is not required. Similar considerations apply to the other lowest generation states. This same criterion for solution was not used in the control calculation shown in column 5 of Table 2, where it has been checked that the two sides of (15) agree to the accuracy indicated.

[11] For a detailed discussion of this fact, see Appendix C of [21].

References

[1] A succinct summary of the features of the standard model of interest in this paper can be conveniently found on the PDG website: http://durpdg.dur.ac.uk/lbl/

[2] N. Steenrod, *The Topology of Fibre Bundles*, Princeton University Press, 1974.

[3] Chan Hong-Mo and Tsou Sheung Tsun, Int. J. Mod. Phys. A27 (2012) 1230002 ; arXiv:1111.3832.

[4] Michael J Baker, Jose Bordes, Chan Hong-Mo and Tsou Sheung Tsun, Int. J. Mod. Phys. A27 (2012) 1250087; arXiv:1111.5591.

[5] See e.g. A. Trautman, "Einstein–Cartan Theory", in *Encyclopaedia of Mathematical Physics*, ed. JP Françoise, GL Naber and Tsou Sheung Tsun, Elsevier (Oxford) 2006.

[6] G. 't Hooft, Acta Phys. Austr., Suppl. **22**, 531 (1980).

[7] Chan Hong-Mo and Tsou Sheung Tsun, Eur. Phys. J. **C52**, 635 (2007), arXiv:hep-ph/0611364.

[8] Michael J Baker, Jose Bordes, Chan Hong-Mo and Tsou Sheung Tsun, Int. J. Mod. Phys. A26 (2011) 2087-2124, arXiv:1103.5615.

[9] N. Cabibbo, Phys. Rev. Lett. 10, 531 (1963); M. Kobayashi and K. Maskawa, Prog. Theor. Phys. 49, 282 (1972).

[10] B. Pontecorvo, Zh. Eksp. Teor. Fiz. 33, 549 (1957) and 34, 247 (1958); Z. Maki, M. Nakagawa and S. Sakata, Progr. Theor. Phys. 28, 870 (1962).

[11] José Bordes, Chan Hong-Mo and Tsou Sheung Tsun, Int. J. Mod. Phys. A25 (2010) 5897-5911; arXiv:1002.3542 [hep-ph].

[12] M. Gell-Mann, P. Ramond and R. Slansky (1979), in Supergravity, edited by P. van Nieuwenhuizen and D.Z. Freedman, North Holland Publ. Co.; P. Minkowski, Phys. Lett. B 67 (1977) 421; R.N. Mohapatra and G. Senjanovic, Phy. Rev. Lett. 44 (1980) 912.

[13] See for example: S. Weinberg, *The Quantum Theory of Fields II* (Cambridge University Press, New York, 1996).

[14] José Bordes, Chan Hong-Mo and Tsou Sheung Tsun, Int. J. Mod. Phys. A24 (2009) 101-112; arXiv:0707.3358.

[15] C. Jarlskog, Z. Phys. **C29**, 491 (1985); Phys. Rev. Lett. **55**, 1039 (1985).

[16] Machacek, M., Vaughn, M., Nucl. Phys. B236 (1985) 221.

[17] Cheng, T., Eichten, E. and Li, Ling-Fong, Phys. Rev. D9 (1974) 2259.

[18] Luo, M., Wang, H. Xiao, Y., Phys. Rev. D67 (2003) 06019.

[19] José Bordes, Chan Hong-Mo, Jakov Pfaudler and Tsou Sheung Tsun, Phys. Rev. D58 (1998) 053006; hep-ph/9802436.

[20] Michael J Baker, Jose Bordes, Chan Hong-Mo and Tsou Sheung Tsun, Eur. Phys. Lett. 102 (2013) 41001, arXiv:1110.5951.

[21] Michael J Baker, Jose Bordes, Chan Hong-Mo and Tsou Sheung Tsun, Int. J. Mod. Phys. A28 (2013) 1350070; arXiv: 1206.0199.

[22] Jose Bordes, Chan Hong-Mo and Tsou Sheung Tsun, Eur. Phys. J. C65; 537-542, 2010; arXiv:0908.1750.

[23] T. Appelquist and J. Carrazone., Phys. Rev.11 (1975) 2586.

[24] CMS Collaboration, CMS-PAS-HIG-13-034, CERN Document Server, dated 2014/03/04.

[25] see e.g. M Davier et al., Eur. Phys. J. C(2008) 56: 305; A. Pich, PoS ConfinementX (2012) 022.